CELL BIOLOGY

TGFBR3L is an inhibin B co-receptor that regulates female fertility

Emilie Brûlé[1], Ying Wang[2], Yining Li[2], Yeu-Farn Lin[2], Xiang Zhou[2], Luisina Ongaro[2], Carlos A. I. Alonso[2], Evan R. S. Buddle[2], Alan L. Schneyer[3], Chang-Hyeock Byeon[4], Cynthia S. Hinck[4], Natalia Mendelev[5], John P. Russell[6], Mitra Cowan[7], Ulrich Boehm[8], Frederique Ruf-Zamojski[5], Michel Zamojski[5], Cynthia L. Andoniadou[6,9], Stuart C. Sealfon[5], Craig A. Harrison[10], Kelly L. Walton[10], Andrew P. Hinck[4], Daniel J. Bernard[1,2]*

Follicle-stimulating hormone (FSH), a key regulator of ovarian function, is often used in infertility treatment. Gonadal inhibins suppress FSH synthesis by pituitary gonadotrope cells. The TGFβ type III receptor, betaglycan, is required for inhibin A suppression of FSH. The inhibin B co-receptor was previously unknown. Here, we report that the gonadotrope-restricted transmembrane protein, TGFBR3L, is the elusive inhibin B co-receptor. TGFBR3L binds inhibin B but not other TGFβ family ligands. TGFBR3L knockdown or overexpression abrogates or confers inhibin B activity in cells. Female *Tgfbr3l* knockout mice exhibit increased FSH levels, ovarian follicle development, and litter sizes. In contrast, female mice lacking both TGFBR3L and betaglycan are infertile. TGFBR3L's function and cell-specific expression make it an attractive new target for the regulation of FSH and fertility.

INTRODUCTION

Fertility is controlled by a complex network of hormones from the brain, pituitary gland, and gonads. Follicle-stimulating hormone (FSH) from pituitary gonadotrope cells promotes gamete maturation through its actions on somatic cells in the gonads (*1*). Recombinant and purified forms of the hormone are mainstays of assisted reproductive technologies (*2*). FSH also stimulates production of gonadal inhibins, which feed back to the pituitary to suppress FSH secretion (*3*, *4*). The mechanisms of inhibin action remain incompletely resolved.

Inhibins are transforming growth factor β (TGFβ) ligands (*5*) consisting of heterodimers of the inhibin α subunit disulfide-linked to either the inhibin βA (inhibin A) or inhibin βB subunit (inhibin B) (*5*, *6*). According to current dogma, inhibins are competitive antagonists of pituitary activins (*7*–*10*). Activins are dimers of the inhibin β subunits that promote FSH transcription (*9*, *11*–*13*) through complexes of activin type I and II receptors (*14*–*17*). To block activin signaling, inhibins competitively bind to activin type II receptors via the β subunits they share with activins (*7*, *10*, *18*, *19*) but do not recruit the signaling type I receptors (*8*). Inhibins interact not only with activin type II receptors but also with the TGFβ type III receptor betaglycan to form high-affinity, ternary complexes (*7*, *18*), thereby robustly suppressing FSH production. While betaglycan functions as an obligate inhibin A co-receptor in gonadotropes, the inhibin B co-receptor had remained elusive (*20*). Here, we demonstrate that the orphan transmembrane protein, TGFβ receptor type III-like (TGFBR3L), is the inhibin B–specific co-receptor. The discovery of this protein suggests a novel means to regulate FSH levels and fertility.

[1]Department of Anatomy and Cell Biology, McGill University, Montreal, Québec, Canada. [2]Department of Pharmacology and Therapeutics, McGill University, Montreal, Québec, Canada. [3]Fairbanks Pharmaceuticals, Concord, MA, USA. [4]Department of Structural Biology, University of Pittsburgh School of Medicine, Pittsburgh, PA, USA. [5]Department of Neurology, Center for Advanced Research on Diagnostic Assays, Icahn School of Medicine at Mount Sinai, New York, NY, USA. [6]Centre for Craniofacial and Regenerative Biology, King's College London, London, UK. [7]McGill Integrated Core for Animal Modeling (MICAM), McGill University, Montreal, Québec, Canada. [8]Department of Experimental Pharmacology, Center for Molecular Signaling, Saarland University School of Medicine, Homburg, Germany. [9]Department of Medicine III, University Hospital Carl Gustav Carus, Technische Universität Dresden, Dresden, Germany. [10]Department of Physiology, Monash Biomedicine Discovery Institute, Monash University, Clayton, Victoria, Australia.
*Corresponding author. Email: daniel.bernard@mcgill.ca

RESULTS

TGFBR3L is selectively expressed in gonadotrope cells

TGFBR3L, a newly identified molecule that shares homology with the membrane-proximal zona pellucida (ZP-C) domain of betaglycan ($BG_{ZP\text{-}C}$), emerged as a promising candidate inhibin B co-receptor when bulk and single-cell RNA sequencing (scRNA-seq) analyses showed *Tgfbr3l* (Gm14378) mRNA enrichment in murine gonadotropes (*21*, *22*). We confirmed these observations in our own scRNA-seq datasets from 10- to 12-week-old C57BL/6 female and male mouse pituitaries (Fig. 1, A and B, and fig. S1, A and B) (*23*). *Tgfbr3l* mRNA is also selectively expressed in rat gonadotropes (*24*), and the TGFBR3L protein was recently reported to be a gonadotrope-specific membrane protein of unknown function in human pituitary (*25*). We similarly observed *TGFBR3L* mRNA enrichment in human gonadotropes in single-nucleus (sn) RNA-seq analyses (Fig. 1, C and D, and fig. S1, C and D) (*26*). In adult mice, *Tgfbr3l* mRNA expression in the pituitary gland far exceeded that of any other tissue examined (Fig. 1E and fig. S1E). Analysis of sn assay for transposase-accessible chromatin with high-throughput sequencing (snATAC-seq) in mouse pituitary identified open chromatin around the 5′ flanking sequence (promoter) and exon 1 of *Tgfbr3l* in gonadotropes but not in other pituitary cell lineages (Fig. 1F and fig. S2). Thus, *Tgfbr3l* expression appears to be pituitary-specific among tissues, which is consistent with the human proteomics atlas survey (*27*). Within the pituitary, *Tgfbr3l* proximal regulatory domain accessibility and expression are gonadotrope cell type specific.

TGFBR3L is a transmembrane glycoprotein

The murine *Tgfbr3l* mRNA is predicted to encode a type I transmembrane protein of 297 amino acids, with an N-terminal signal peptide, a single extracellular ZP domain, a transmembrane domain, and a short intracellular carboxy-terminal tail (Fig. 2A). The ZP

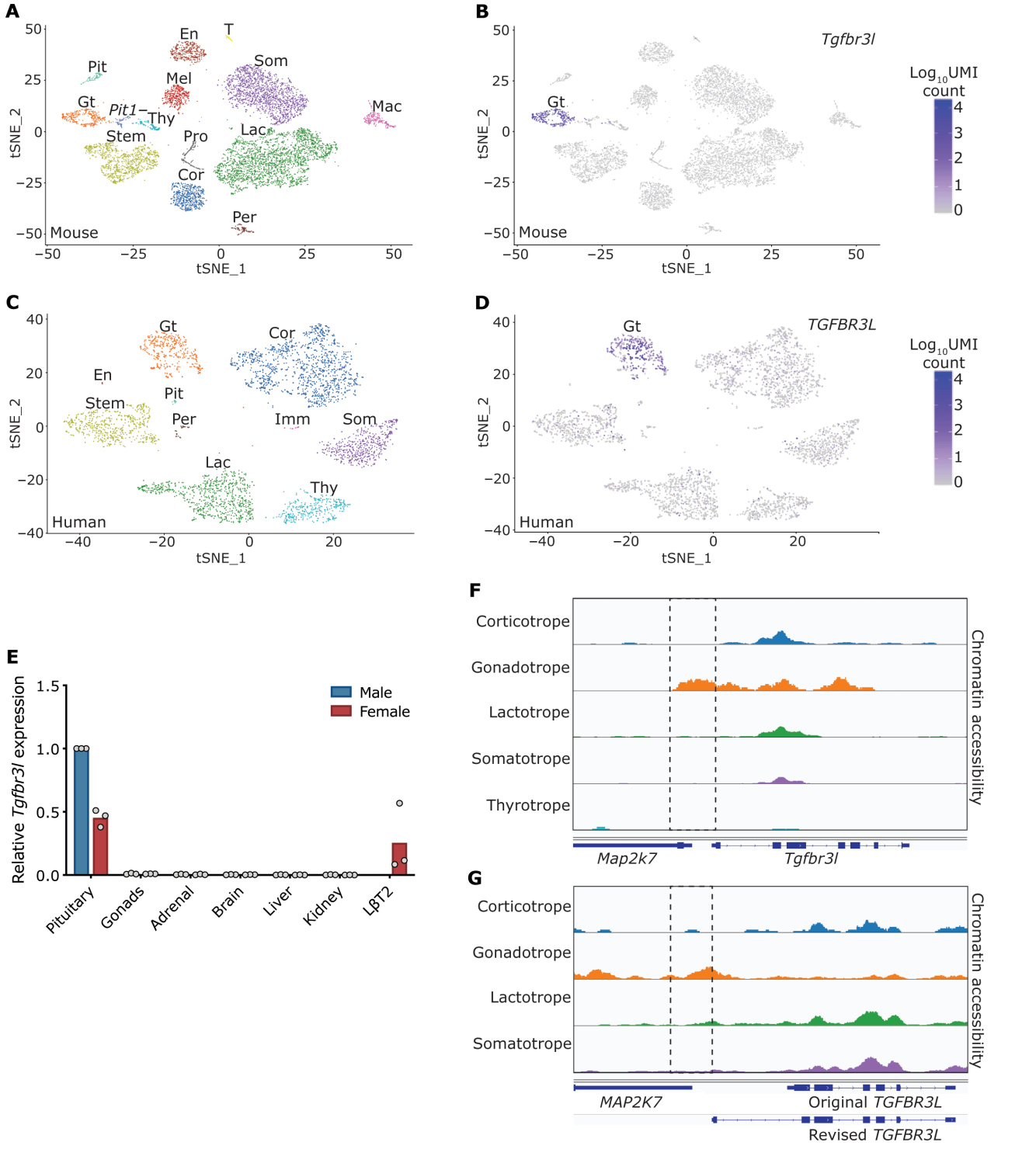

Fig. 1. *Tgfbr3l*/*TGFBR3L* is specifically expressed in pituitary gonadotrope cells. (**A** and **C**) t-Distributed stochastic neighbor embedding (t-SNE) representations of scRNA-seq of female murine and snRNA-seq of female human pituitaries. Different colored clusters represent different pituitary cell types, which are labeled above the clusters: corticotropes (Cor), endothelial cells (En), gonadotropes (Gt), immune cells (Imm), lactotropes (Lac), macrophages (Mac), melanotropes (Mel), pericytes (Per), pituicytes (Pit), *Pit1* negative thyrotropes (*Pit1*–), proliferating (Pro), somatotropes (Som), stem cells (Stem), T cells (T), and thyrotropes (Thy). (**B** and **D**) Feature plots of *Tgfbr3l*/*TGFBR3L* expression. UMI, Unique Molecular Identifier. (**E**) *Tgfbr3l* expression in 8-week-old male (blue) and female (red) mouse tissues and in gonadotrope-like LβT2 cells. Expression was normalized to male pituitary. *Rpl19* was used as a housekeeping gene. (**F** and **G**) Chromatin accessibility plots from snATAC-seq of male murine and human pituitaries. The dotted box indicates the promoter regions of *Tgfbr3l*/*TGFBR3L*. Note that few nuclei were isolated from the male human pituitary; therefore, only the four cell types shown in (G) could be identified conclusively.

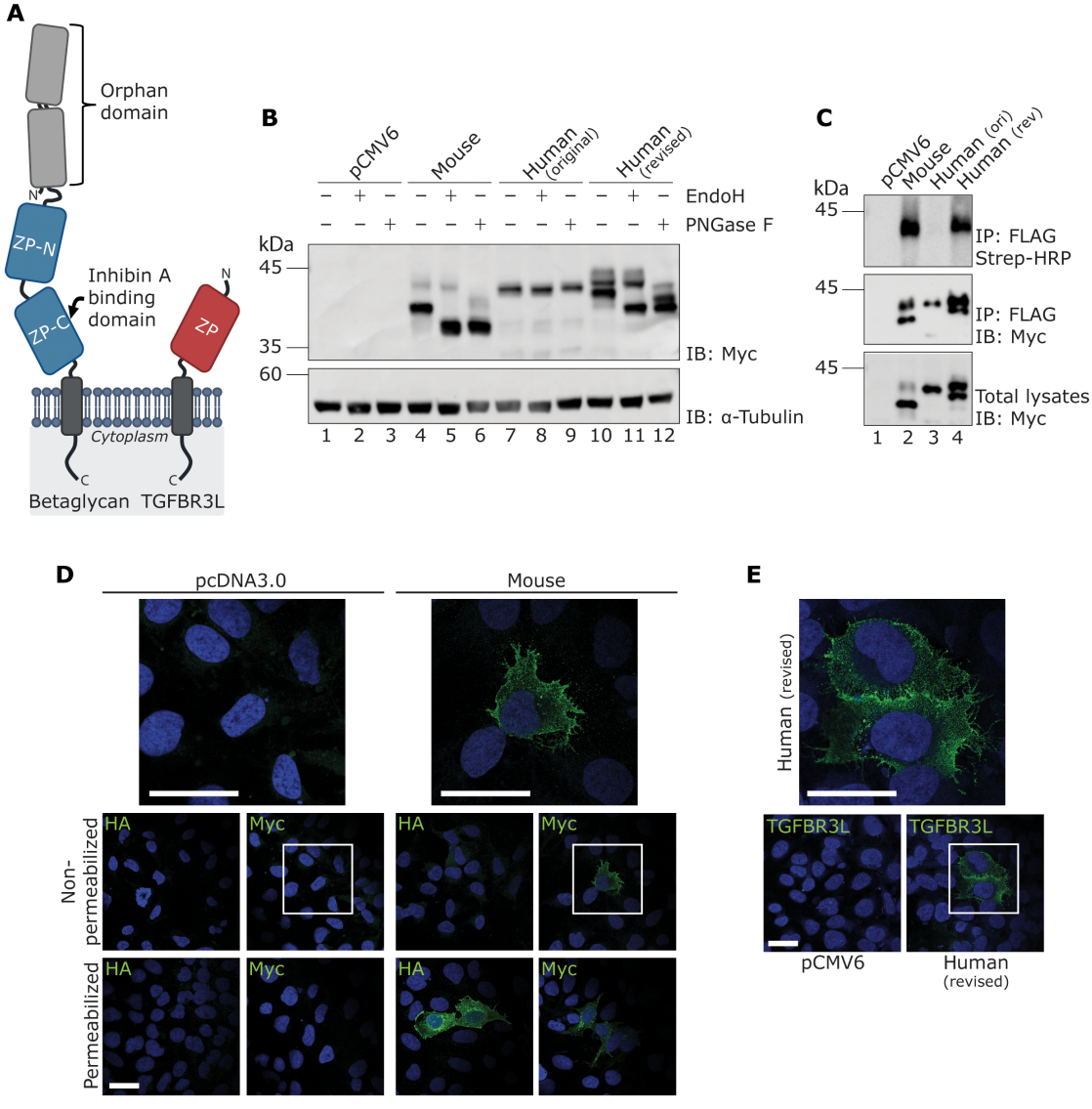

Fig. 2. TGFBR3L is a transmembrane glycoprotein. (**A**) Schematic representation of betaglycan and TGFBR3L. Betaglycan has four subdomains in its ECD (two orphan domains and two ZP domains), a transmembrane domain, and a cytoplasmic tail. The inhibin A binding domain (ZP-C) is indicated by an arrow. TGFBR3L has a single extracellular ZP domain, a transmembrane domain, and a cytoplasmic tail. (**B**) Protein lysates from HEK293T cells transfected with pCMV6, murine TGFBR3L-Myc-DDK, and original (ori) or revised (rev) human TGFBR3L-Myc-DDK either untreated or treated with Endo H or PNGase F and immunoblotted (IB) against c-Myc. α-Tubulin was used as a loading control. (**C**) HEK293 cells transfected with the same constructs as in (B) subjected to cell surface biotinylation. Protein lysates were either immunoblotted against c-Myc (bottom) or immunoprecipitated (IP) with FLAG and immunoblotted against c-Myc (middle). Membrane expression was analyzed with streptavidin–horseradish peroxidase (strep-HRP) after FLAG IP (top). (**D**) HEK293 cells transfected with either pcDNA3.0 or murine Myc-TGFBR3L-HA. Expression was visualized by immunofluorescence against either c-Myc or HA under nonpermeabilizing or permeabilizing conditions. Nuclei were stained with DAPI (blue). Boxed regions are magnified above. (**E**) HEK293 cells were transfected with pCMV6 or the revised human TGFBR3L-Myc-DDK and visualized by immunofluorescence under nonpermeabilizing conditions using an antibody against the N terminus of human TGFBR3L. Scale bars, 50 μm.

domain is ~33% identical to $BG_{ZP\text{-}C}$ in both mouse and human (fig. S3, A and B). Inhibin A binds to $BG_{ZP\text{-}C}$ but not to other domains of betaglycan (*28*, *29*). When ectopically expressed in heterologous cells, murine TGFBR3L migrated as a doublet of 38 to 42 kDa on SDS–poly-acrylamide gel electrophoresis (SDS-PAGE) (Fig. 2B, lane 4). The upper and lower bands reflect mature [endoglycosidase H (Endo H)–insensitive] and immature (EndoH-sensitive) glycoforms, respectively (Fig. 2B, lanes 5 and 6). Only the mature form was observed at the plasma membrane, as revealed by cell-surface biotinylation (Fig. 2C, lane 2). This form of the protein corresponds in size to a previously unidentified protein that bound inhibin B but not inhibin A in the murine gonadotrope-like cell line, LβT2 (*30*). We confirmed *Tgfbr3l* mRNA expression in these cells (Fig. 1E).

When we expressed human TGFBR3L in heterologous cells using a commercially sourced expression vector (OriGene), the protein was not glycosylated (Fig. 2B, lanes 7 to 9) and did not reach the cell membrane (Fig. 2C, lane 3). It is important to note, however, that the human TGFBR3L coding sequence in this vector and in publicly

available databases (NCBI NM_001195259) was computationally rather than experimentally determined and lacked a signal peptide. In addition, we questioned the accuracy of the predicted first exon. Using rapid amplification of complementary DNA (cDNA) (RACE) to map the 5′ end of *TGFBR3L* in human pituitary, we identified a different exon 1 that both corresponded to exon 1 in mice and encoded a signal peptide (fig. S4; GenBank accession no. MW464126). As shown in snATAC-seq data, there is a peak of open chromatin immediately upstream of this exon in human gonadotropes, but not in other pituitary cell lineages (Fig. 1G). When expressed in heterologous cells, the revised human TGFBR3L was a cell-surface glycoprotein, as observed with the mouse protein (Fig. 2B, lanes 10 to 12; and Fig. 2C, lane 4). Membrane localization of both the murine (Fig. 2D) and human (Fig. 2E) TGFBR3L was confirmed by immunofluorescence in transfected cells.

TGFBR3L mediates inhibin B actions in cells

We hypothesized that TGFBR3L may function as an inhibin B co-receptor given that it (i) is enriched in gonadotropes; (ii) is a transmembrane protein; (iii) has sequence identity to $BG_{ZP\text{-}C}$, the only domain of betaglycan that binds inhibins (*28*); and (iv) is similar in size to the previously unidentified inhibin B binding protein in LβT2 cells (*30*). Consistent with this hypothesis, inhibin B, but not inhibin A, antagonism of activin A signaling was enhanced in heterologous Chinese hamster ovary (CHO) cells stably expressing murine (Fig. 3, A and B) or human TGFBR3L (fig. S5, A and B). In contrast, CHO cells stably expressing betaglycan showed enhanced sensitivity to both inhibins (Fig. 3, A and B). Comparable results were observed in heterologous COV434 cells transiently expressing the murine TGFBR3L (fig. S5, C and D).

In homologous LβT2 cells, inhibins B and A antagonized activin A signaling (Fig. 3, C to F). The inhibin A (Fig. 3D), but not inhibin B (Fig. 3C), response was blocked by small interfering RNA (siRNA)–mediated knockdown of betaglycan. This difference between ligands was similar to what was observed in inhibin A– or B–treated pituitary cultures from gonadotrope-specific betaglycan knockout (KO) mice (*20*). In contrast, knocking down TGFBR3L with siRNAs (fig. S5E) significantly attenuated inhibin B's antagonism of activin A–stimulated reporter activity (Fig. 3E), but had no effect on inhibin A (Fig. 3F). Inhibin B action was fully blocked when siRNAs against betaglycan and TGFBR3L were cotransfected (fig. S5F). These results suggest that in gonadotrope-like cells: (i) inhibin A acts via betaglycan, (ii) inhibin B acts via TGFBR3L in the presence or absence of betaglycan, and (iii) betaglycan can mediate some of inhibin B's actions in the absence of TGFBR3L.

Inhibin B binds TGFBR3L with high affinity and specificity

We next used surface plasmon resonance (SPR) to examine TGFBR3L binding to different TGFβ ligands. We immobilized inhibin A, inhibin B, or TGFβ2 on sensor chips and used recombinant forms of the extracellular domains (ECDs) of the human activin type IIA receptor (ActRII), rat betaglycan ($BG_{ZP\text{-}C}$), and murine TGFBR3L as analytes. Inhibins A and B but not TGFβ2 bound to ActRII with nanomolar affinity (Fig. 4, A to C, and table S1). The inhibin-binding affinities for ActRII were comparable to that of immobilized activin A (fig. S6 and table S1). TGFβ2 bound strongly to $BG_{ZP\text{-}C}$ (Fig. 4D and table S1), whereas inhibin A bound with lower affinity (Fig. 4E and table S1). Inhibin B binding to $BG_{ZP\text{-}C}$ was too weak to accurately quantify in these assays (Fig. 4F and tables S1). As anticipated, TGFBR3L bound inhibin B with high affinity (K_d, 52 nM; Fig. 4I and table S1), but not inhibin A (Fig. 4H and table S1) or TGFβ2 (Fig. 4G and table S1).

Female *Tgfbr3l* KO mice exhibit enhanced ovarian folliculogenesis and fertility

To assess TGFBR3L function in vivo, we generated *Tgfbr3l* KO mice using CRISPR-Cas9 (Fig. 5, A and B). We focused on females in our analyses, as inhibins do not play major physiological roles in adult male mice (fig. S7), in contrast to male humans and nonhuman primates (*20*, *31*–*34*). Puberty onset, estrous cyclicity, and body weights were similar in KO and wild-type (WT) females (fig. S8, A to C). In breeding trials, KO females had increased litter sizes relative to WT (Fig. 5C), although litter frequency was normal (fig. S8D). KOs showed increased numbers of antral follicles (Fig. 5, D to F) and corpora lutea (Fig. 5, D to E and G), although their ovarian and uterine weights were normal (fig. S8, E to F), as was aromatase (*Cyp19a1*) and inhibin subunit expression in their ovaries (fig. S8G). Serum inhibin A and B levels did not differ between genotypes (fig. S8I). Relative to WT, KOs ovulated more eggs in natural cycles (Fig. 5H) and showed increased uterine implantation sites (Fig. 5I). When treated with exogenous gonadotropins, the two genotypes ovulated similar numbers of eggs, ruling out inherent differences in ovarian function (fig. S8H).

These phenotypes would be expected if inhibin B negative feedback was impaired, leading to enhanced FSH secretion. FSH is a dimer of the FSHβ subunit (product of the *FSHB*/*Fshb* gene) noncovalently linked to the glycoprotein hormone α subunit (CGA), which it shares with luteinizing hormone (LH) (*35*). Inhibins suppress *Fshb* expression, without affecting *Cga* or the LHβ subunit (*Lhb*) (*4*, *36*). We observed modest increases in serum FSH (Fig. 5J) and pituitary *Fshb* mRNA levels (Fig. 5K) in KO females sampled on diestrus relative to WT, but these differences were not statistically significant in this cohort. Serum progesterone (P4; fig. S8J), serum LH (fig. S8K), and pituitary expression of *Lhb*, *Cga*, and the gonadotropin-releasing hormone receptor (*Gnrhr*) were unaltered in KOs (fig. S8L). As expected, *Tgfbr3l* mRNA levels were significantly depleted in KO relative to WT pituitaries (Fig. 5, B and K). In contrast, steroidogenic factor 1 (*Nr5a1*), a lineage-specific transcription factor, was expressed at normal levels, suggesting that gonadotrope development was unaltered in the KO mice (Fig. 5K). Cultured pituitaries from KOs showed a small but nonsignificant decrease (rightward shift) in inhibin B suppression of *Fshb* expression relative to WT (fig. S8M). Inhibin A sensitivity was modestly increased in KO pituitaries (fig. S8N).

Overall, *Tgfbr3l* KO mice exhibited phenotypes similar to those observed in mice lacking betaglycan in gonadotrope cells (*20*). These results and those observed in knockdown cells (Fig. 3E and fig. S5F) suggested that the deletion of both co-receptors might be required to more fully abrogate inhibin B action. Consistent with this idea, FSH levels increased in diestrus KO females following treatment with anti-inhibin serum (AIS), indicating that their pituitaries retained sensitivity to endogenous inhibins in the absence of TGFBR3L (fig. S8O).

Tgfbr3l/betaglycan dKO mice have markedly elevated FSH levels

We next generated mice with a global KO of *Tgfbr3l* and gonadotrope-specific deletion of betaglycan ($Gnrhr^{Cre/+}$;$Tgfbr3^{fl/fl}$;$Tgfbr3l^{-/-}$; hereafter double KOs or dKOs). Global betaglycan KO mice are not

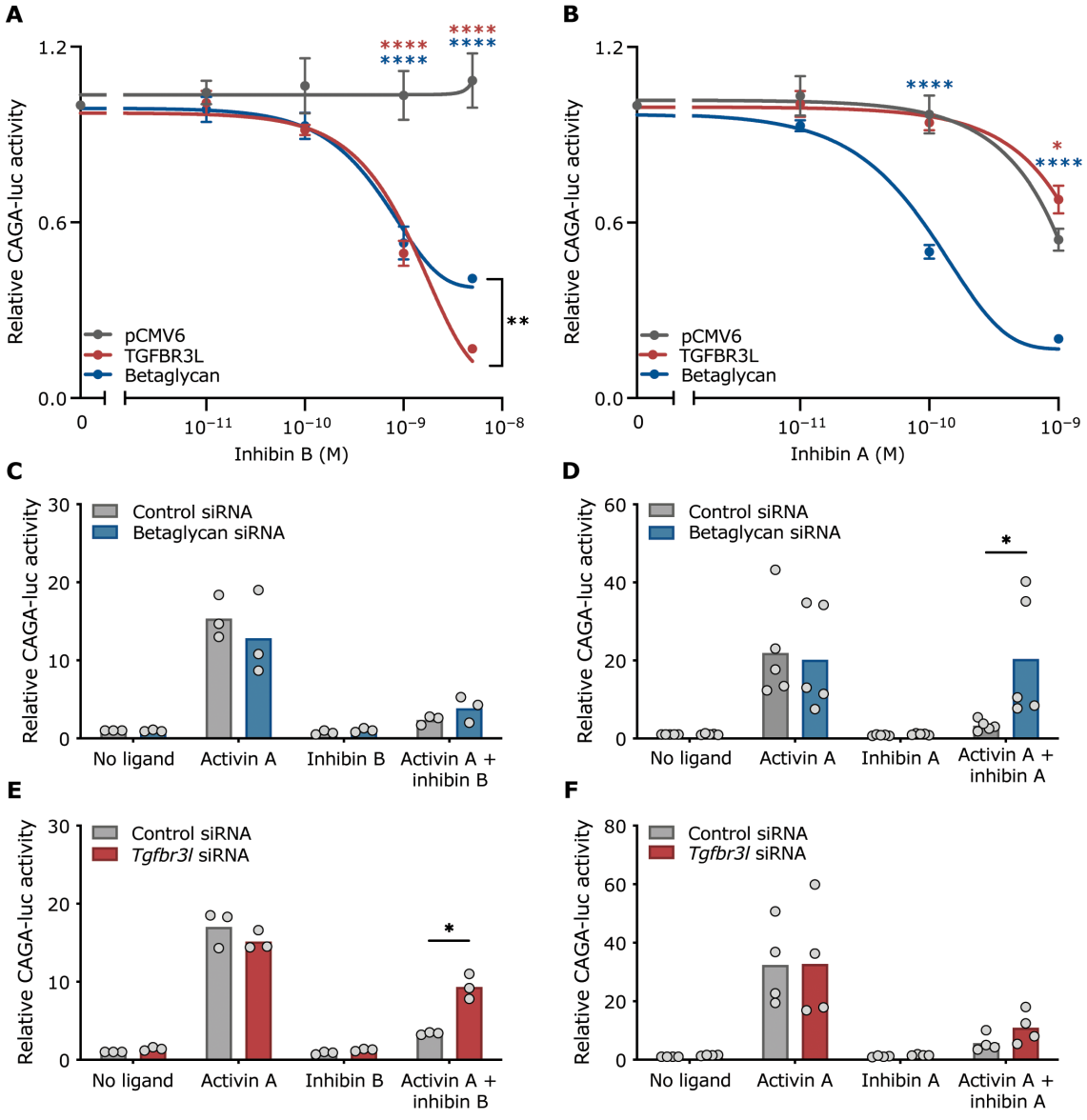

Fig. 3. TGFBR3L mediates inhibin B actions in vitro. (**A** and **B**) Inhibin sensitivity of three different CHO cell lines generated with either stable integration of pCMV6 (gray), murine TGFBR3L-Myc-DDK (red), or rat Myc-betaglycan (blue). Stable cells were transfected with the CAGA-luc reporter plasmid and treated with 1 nM activin A and the indicated concentration of inhibin B (AnshLabs; A) or inhibin A (R&D Systems, B). (**C** to **F**) LβT2 cells were transfected with the CAGA-luc reporter plasmid and 2 nM of control (gray), betaglycan (blue), or *Tgfbr3l* (red) siRNA. Cells were either left untreated or treated with 1 nM activin A and/or 1 nM inhibin B (R&D Systems, C and E) or 1 nM inhibin A (R&D Systems, D and F). Data represent mean values (±SEM) from three to five independent experiments. Data were analyzed by two-way ANOVA, followed by Tukey's (A and B) or Sidak's (C to F) multiple comparisons tests. *$P < 0.05$, **$P < 0.01$, and ****$P < 0.0001$.

viable (*37*). The genetic cross used to produce these dKO mice also yielded littermates with different extents of *Tgfbr3l* inactivation, which we included as controls (fig. S9). The first (*Gnrhr*$^{+/+}$;*Tgfbr3*$^{fl/fl}$;*Tgfbr3l*$^{+/-}$; hereafter *Tgfbr3l*$^{+/-}$) were ostensibly heterozygous *Tgfbr3l* KO mice, which do not exhibit alterations in FSH synthesis or secretion (fig. S10). These mice were used in some but not all analyses. The second control strain (*Gnrhr*$^{+/+}$;*Tgfbr3*$^{fl/fl}$;*Tgfbr3l*$^{-/-}$; hereafter *Tgfbr3l*$^{-/-}$) is equivalent to the *Tgfbr3l* KOs described in Fig. 5 and was the primary control group used in the following experiments. The third control strain, which we did not fully characterize (*Gnrhr*$^{Cre/+}$;*Tgfbr3*$^{fl/fl}$;*Tgfbr3l*$^{+/-}$), most resembled *Tgfbr3l*$^{+/-}$. As with the single KOs described above, we focused our analyses on females (although see male data in fig. S11).

Puberty onset, estrous cyclicity, and body weights did not differ between genotypes (fig. S12, A to C). However, dKO females had markedly increased serum FSH, pituitary FSH protein content, and pituitary *Fshb* mRNA levels relative to controls (Fig. 6, A to C). LH levels and expression of *Lhb*, *Cga*, and *Nr5a1* did not differ between genotypes (fig. S12, D and E). *Gnrhr* expression was increased in dKO females (fig. S12E), consistent with previous observations in gonadotrope-specific betaglycan KO mice (*20*). In this cohort of animals, FSH levels were also significantly increased in *Tgfbr3l*$^{-/-}$ relative

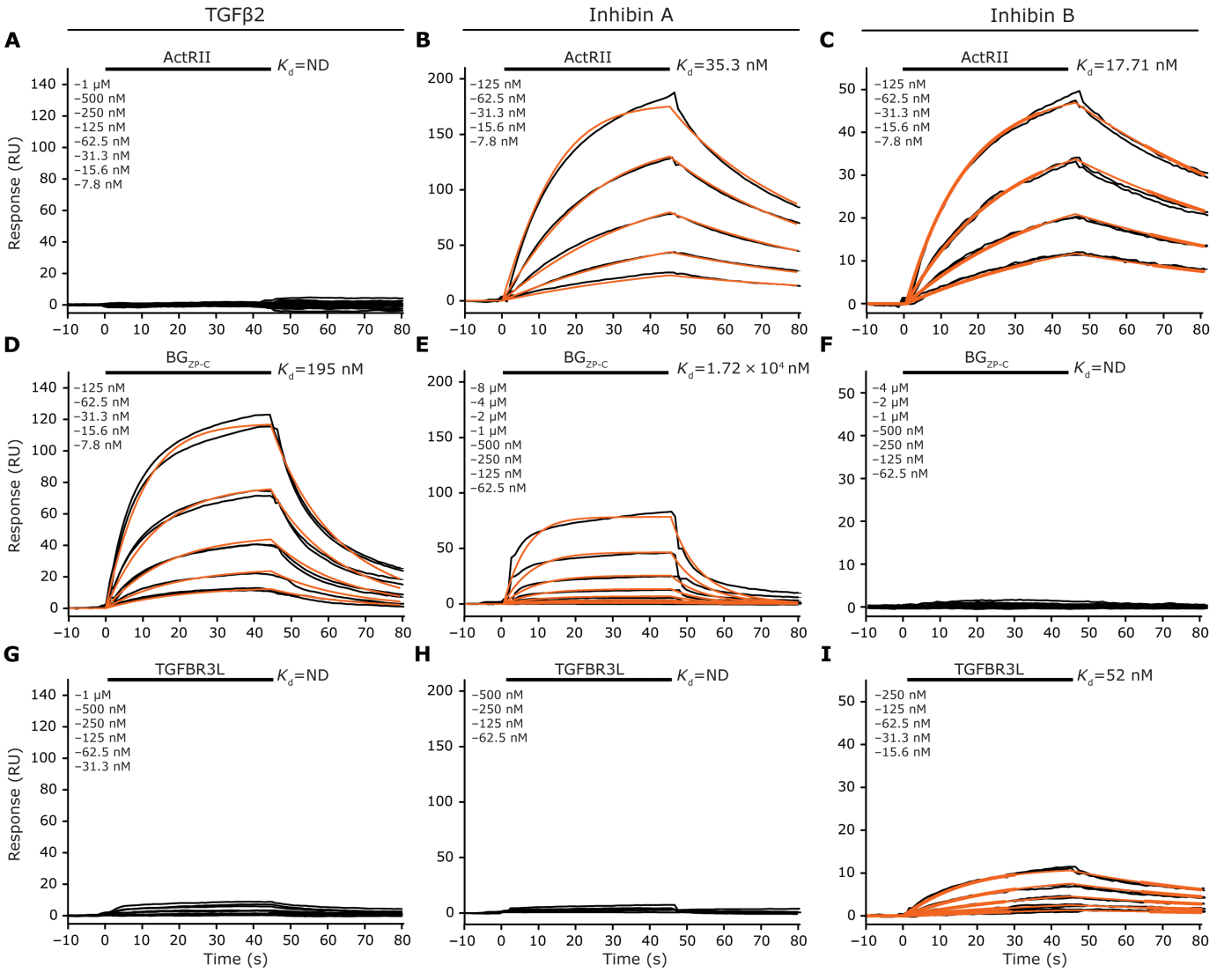

Fig. 4. TGFBR3L binds inhibin B with high affinity and specificity. SPR sensorgrams of ActRII (**A** to **C**), BG_{ZP-C} (**D** to **F**), and TGFBR3L (**G** to **I**) binding to immobilized TGFβ2 (left column), inhibin A (middle column), and inhibin B (right column). Concentrations of receptors used are indicated in the top left corner of each graph. Kinetic fits are shown in orange over experimental curves in black. ND, could not be determined.

to *Tgfbr3l*$^{+/-}$ females (Fig. 6, A to C). In contrast, there was no effect on FSH release in male dKOs (fig. S11E). dKO females had significantly larger ovaries than *Tgfbr3l*$^{-/-}$ controls (Fig. 6, D to F), which was associated with marked increases in numbers of antral follicles (Fig. 6, E to G); corpora lutea (Fig. 6, E, F, and H); *Cyp19a1*, *Inha*, *Inhba*, and *Inhbb* expression (Fig. 6I); serum inhibins A and B (Fig. 6J); serum P4 (Fig. 6K); and oocytes ovulated in natural cycles (Fig. 6L). Uterine weights were also increased in dKO mice (Fig. 6M). Nevertheless, dKO females did not produce live offspring (Fig. 6N) in breeding trials. The nature of the fertility defect will be reported elsewhere.

Pituitaries of *Tgfbr3l*/betaglycan dKO mice are insensitive to inhibins

Last, we assessed gonadotrope sensitivity to inhibins in dKO mice. We treated pituitary cultures from *Tgfbr3l*$^{-/-}$ and dKO mice with inhibin A or B. Whereas both inhibins suppressed *Fshb* mRNA expression in *Tgfbr3l*$^{-/-}$ cultures in a concentration-dependent manner, these effects were blocked in dKO pituitaries (Fig. 7, A and B). These data show that inhibin sensitivity was greatly impaired in pituitaries of dKO mice.

DISCUSSION

The data demonstrate that TGFBR3L functions as an inhibin B co-receptor. We show that TGFBR3L is a transmembrane glycoprotein restricted in its expression to pituitary gonadotrope cells of mice and humans that binds inhibin B with high affinity and specificity. Gonadotropes are the canonical inhibin B target cells. Genetic deletion of *Tgfbr3l* leads to increases in FSH levels and ovarian folliculogenesis and thereby to enhanced fecundity in female mice. These data not only uncover new biology in the TGFβ family and in the endocrine control of reproduction but also identify a novel target for the regulation of endogenous FSH levels and the treatment of reproductive disorders.

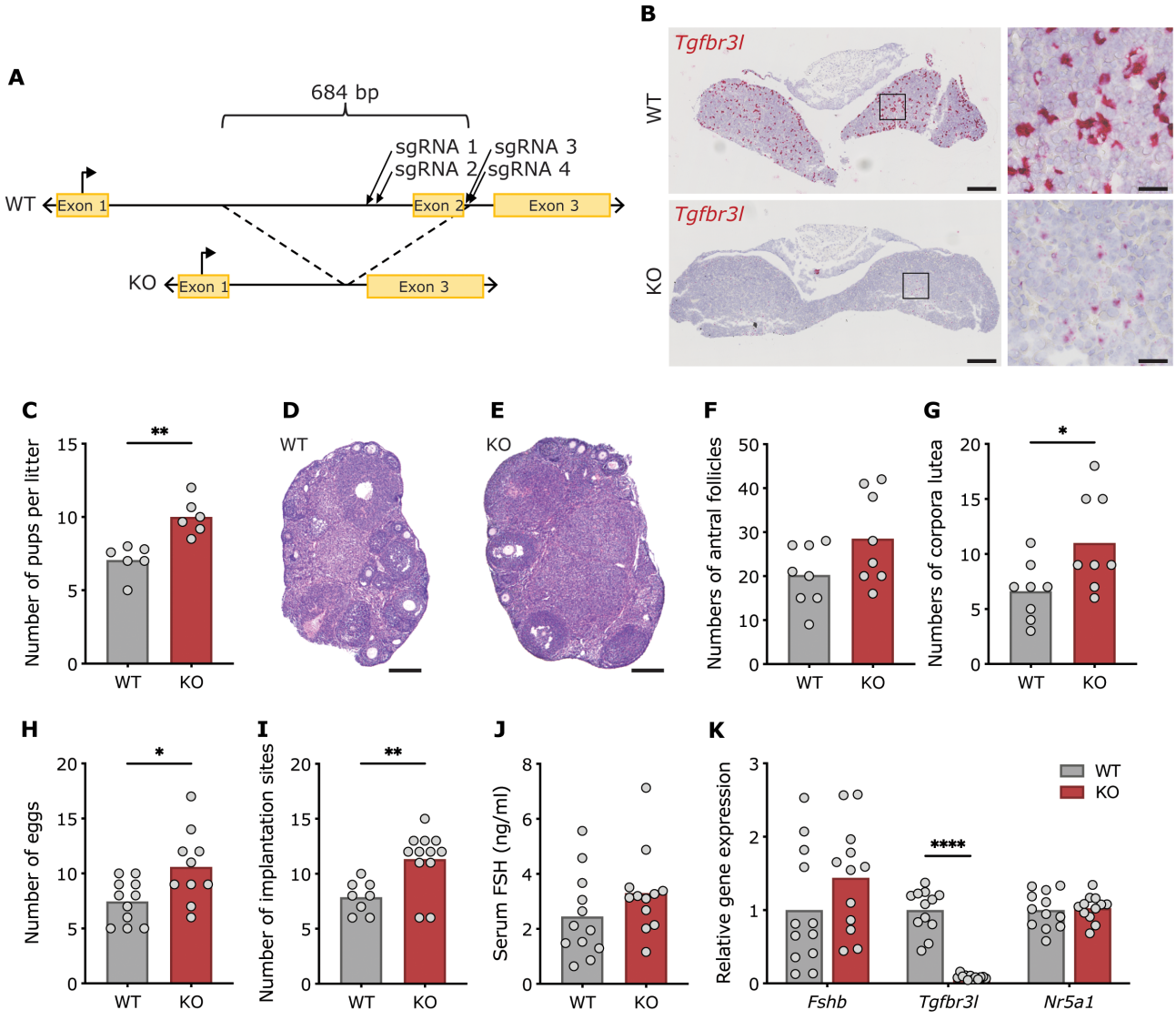

Fig. 5. *Tgfbr3l* KO females have increased fertility. (**A**) Global *Tgfbr3l* KO mice were generated with CRISPR-Cas9. Four sgRNAs were used to target introns 1 and 2 and excise exon 2. The resulting KO (KO) mouse line harbors a 684-bp deletion including exon 2. (**B**) mRNA in situ hybridization (RNAscope) against *Tgfbr3l* (red) on pituitary sections from WT or KO 8-week-old male mice. Boxed regions (left) are magnified (right). Scale bars, 200 and 50 μm. (**C**) Number of pups per litter in 6-month breeding trials. Representative ovarian histology with hematoxylin and eosin (H&E) staining from WT (**D**) and KO (**E**). Scale bars, 200 μm. Antral follicles (**F**) and corpora lutea (**G**) counts from ovarian sections. (**H**) Number of eggs ovulated in natural cycles. (**I**) Number of uterine implantation sites at 5.5 dpc. (**J**) Serum FSH and (**K**) pituitary mRNA expression of *Fshb*, *Tgfbr3l*, and *Nr5a1*. *Rpl19* was used as a housekeeping gene. Data in (D) to (G) and (J) and (K) were collected from 9-week-old females on the morning of diestrus. Each dot on the graphs represents an individual female. Data were analyzed by a two-tailed unpaired *t* test with Welch's correlation. $^{*}P < 0.05$, $^{**}P < 0.01$, and $^{****}P < 0.0001$.

Inhibins A and B are distinct hormones but were generally thought to function equivalently as high-affinity activin type II receptor antagonists in the presence of betaglycan (*7*, *38*). Nevertheless, this notion was challenged by previous observations. In particular, inhibin B more potently suppresses FSH than inhibin A in rats but has a lower affinity for betaglycan in vitro (*30*). Moreover, inhibin B, but not inhibin A, can suppress FSH in gonadotrope-specific betaglycan KO mice (*20*). The discovery and characterization of TGFBR3L explain both inhibin B's greater potency and its sustained activity in the absence of betaglycan in gonadotropes. The data also show that inhibin B can act via betaglycan in the absence of TGFBR3L, which may help explain the hormone's activity in other contexts given betaglycan's broad expression. However, we cannot discount the possibility that alternative co-receptors may mediate inhibin subtype-specific actions in different cell types. Uncharacterized inhibin binding proteins have been observed in gonadal, adrenal, and bone cells (*39*–*41*).

The identification of TGFBR3L inspires new questions. For example, why evolve a cell-specific co-receptor for inhibin B? While we lack a definitive answer, it is tempting to speculate. With some exceptions, adult male mammals only produce inhibin B (*42*, *43*). Inhibin B is the relevant form of the hormone during the follicular phase of the menstrual cycle in women and during metestrus/diestrus in female rodents (*44*, *45*). Therefore, there may be selective pressure

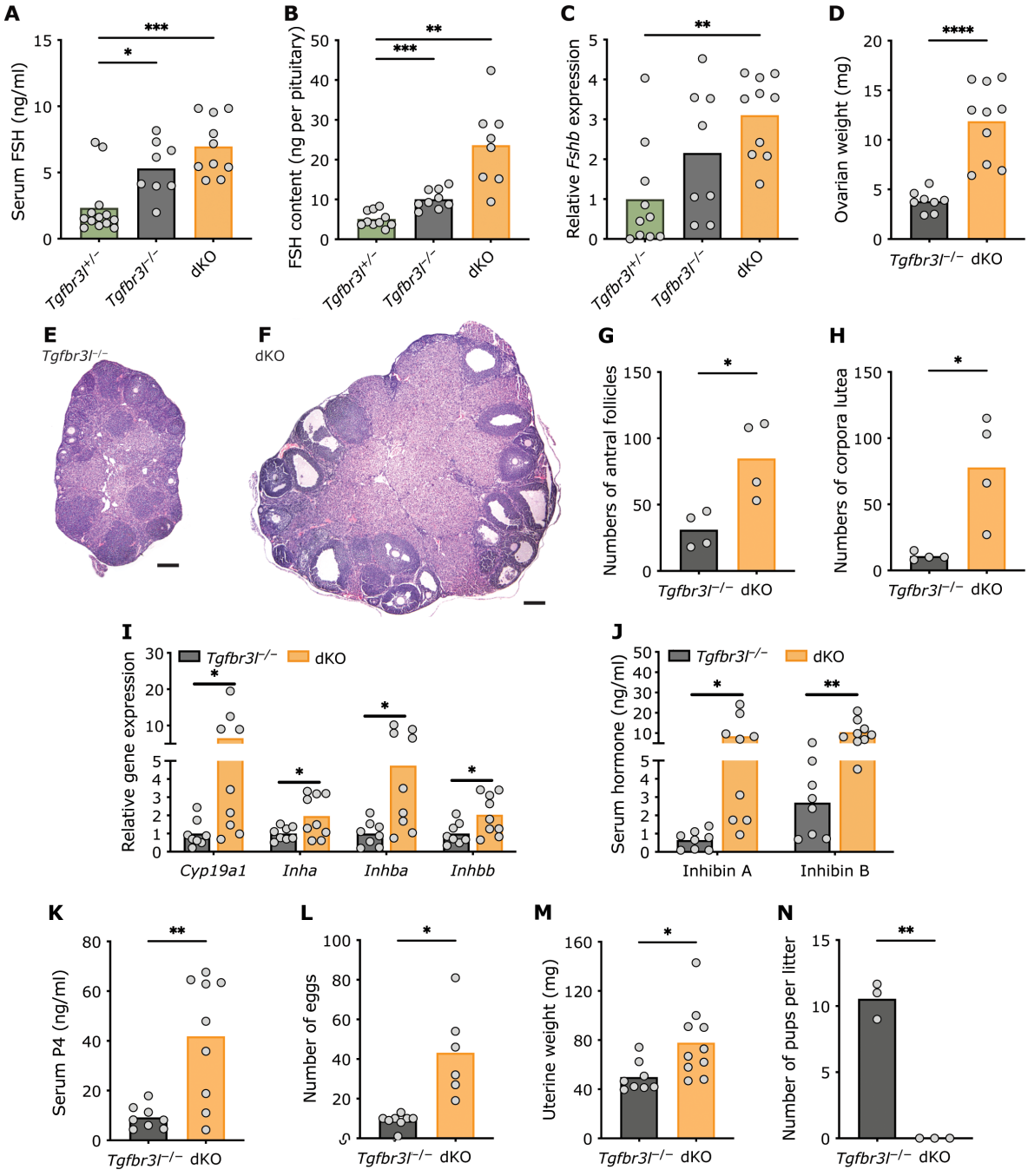

Fig. 6. *Tgfbr3l*/betaglycan dKO females have increased FSH. (**A**) Serum FSH, (**B**) pituitary FSH content, and (**C**) pituitary *Fshb* expression in control [*Tgfbr3l*$^{+/-}$ (green) and *Tgfbr3l*$^{-/-}$ (gray)] and *Tgfbr3l*/betaglycan dKO (yellow) females. (**D**) Ovarian weights and (**E** and **F**) representative ovarian histology with H&E staining from *Tgfbr3l*$^{-/-}$ and dKO mice. Scale bars, 200 μm. Antral follicle (**G**) and corpora lutea (**H**) counts from ovarian sections. (**I**) Ovarian *Cyp19a1*, *Inha*, *Inhba*, and *Inhbb* expression. (**J**) Serum inhibin A and inhibin B levels. (**K**) Serum P4 levels. (**L**) Number of eggs ovulated in natural cycles. (**M**) Uterine weights. (**N**) Number of live pups per litter in a 3-month breeding trial. Data in (A), (C) to (J), and (M) were collected from 9-week-old females on the morning of diestrus. Data in (B) were collected from 9-week-old randomly cycling females. Each dot on the graphs represents an individual female. Data in (A) to (C) were analyzed by Brown-Forsythe and Welch's one-way ANOVA, followed by Dunnett's T3 multiple comparisons test. Data in all other panels were analyzed by two-tailed unpaired *t* test with Welch's correlation. **P* < 0.05, ***P* < 0.01, ****P* < 0.001, and *****P* < 0.0001.

to express a protein that confers inhibin B sensitivity. Whereas betaglycan can serve this function, inhibin B binds betaglycan with lower affinity than inhibin A or the TGFβ isoforms (*7*, *18*, *30*, *46*–*49*). TGFBR3L enables inhibin B to act with high affinity and without competition by other TGFβ family members. Murine gonadotropes do not express the TGFβ type II receptor and therefore cannot transduce signals by TGFβs (*50*, *51*). However, TGFβs can still bind betaglycan in this context and thereby competitively antagonize

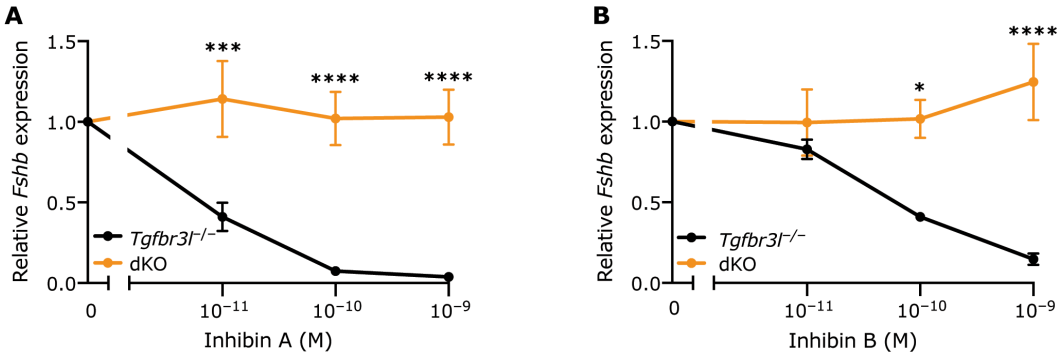

Fig. 7. *Tgfbr3l*/betaglycan dKO pituitaries are insensitive to inhibins. Inhibin sensitivity in pituitary cells cultured from 9- to 13-week-old *Tgfbr3l*$^{-/-}$ (gray) and dKO (yellow) males. Cells were treated with the indicated concentrations of (**A**) inhibin A (R&D Systems) and (**B**) inhibin B (AnshLabs). Twenty-four hours after treatment, *Fshb* mRNA expression was measured by reverse transcription quantitative PCR. *Rpl19* was used as a housekeeping gene. Data represent mean values (± SEM) from three independent experiments. Data were analyzed by two-way ANOVA, followed by Sidak's multiple comparisons test. *$P < 0.05$, ***$P < 0.001$, and ****$P < 0.0001$.

inhibin A (and presumably inhibin B) actions (*52*, *53*). TGFBR3L, which does not bind TGFβ2, and presumably not TGFβ1 or TGFβ3 (75 to 80% sequence identity with TGFβ2), provides inhibin B with the means to bypass this antagonism.

Another intriguing but unanswered question is what explains TGFBR3L's specificity for inhibin B. The inhibin α subunit is assumed to play a major role in inhibin (A and B) binding to the $BG_{ZP\text{-}C}$ (*3*, *28*, *29*, *54*–*56*). Residues in the concave, inward-facing surface of the extended finger region of TGFβ2 contribute to its binding to $BG_{ZP\text{-}C}$ (*29*). On the basis of sequence conservation, the corresponding surface of inhibin α is likely involved in its binding to betaglycan. The relevant residues are not conserved in other members of the TGFβ family (*29*). Given the sequence identity between $BG_{ZP\text{-}C}$ and the ZP domain of TGFBR3L ($TGFBR3L_{ZP}$) (fig. S3), it is possible that inhibin B, through its α subunit, might bind to the latter in a similar fashion. However, as TGFβ2 does not bind $TGFBR3L_{ZP}$, alternative or additional residues must contribute to the interaction. Moreover, as inhibins A and B share the same α subunit, either differences in the conformation of the dimers or in critical residues in their β subunits must explain inhibin B's selectivity for $TGFBR3L_{ZP}$. We previously speculated that sequence differences in the wrist helix regions of the inhibin β subunits likely contribute to inhibin A's higher affinity for $BG_{ZP\text{-}C}$ [fig. S13, (*3*)]. This may also be the case with inhibin B binding to $TGFBR3L_{ZP}$. Structure-function analyses will be critical to determining the nature of these different binding modes.

Inhibins A and B were active at picomolar concentrations in the presence of their respective co-receptors in cells (e.g., Figs. 3, A and B, and 7, A and B). In contrast, the SPR-determined K_ds for the co-receptor–ligand interactions were in the nanomolar range (Fig. 4 and table S1). These apparent affinity differences could be explained by hindrance of binding caused by the direct immobilization of the ligands to the sensor surface. We consider an alternative explanation to be more likely, however. The inhibitory activity of inhibins on cells likely reflects bivalent binding with membrane-localized receptors; that is, the ligands can simultaneously bind the co-receptor and the type II receptor (ActRII or ActRIIB) on the plasma membrane. This type of multivalent membrane-localized assembly has been previously noted for signaling complexes of bone morphogenetic proteins with their type I and type II receptors and has an essential role in increasing potency (*57*). In the absence of a co-receptor, inhibins A and B are unable to effectively compete with activins for binding to cell surface ActRII or ActRIIB (*58*). Nevertheless, in the SPR-binding studies we report here, with immobilized ligands and injected receptor ECD, the affinities of inhibins A and B for ActRII are comparable to that of activin A. Similar results were previously reported for ActRIIB binding to immobilized activin A and inhibin A (*59*). Thus, the reduced ability of inhibins to compete with activins for binding to cell surface ActRII is likely a consequence of avidity rather than an intrinsically lower binding affinity. Inhibins A and B bind monovalently, engaging a single molecule of ActRII, whereas activins bind bivalently or with even greater valency, owing to their ability to simultaneously engage two type II receptor molecules, as well as possibly two type I receptors (*7*, *60*, *61*). Therefore, the picomolar activity of inhibins in cells most likely reflects their simultaneous engagement of a type II receptor and a co-receptor, which they bind individually with nanomolar affinities (*7*, *18*, *30*, *46*).

Last, it is evident that several aspects of TGFBR3L make it a promising new therapeutic target. First, TGFBR3L is highly restricted in its expression; it appears to be unique to pituitary gonadotropes. Although we did not examine all cell types in mice, it is clear from the data presented here and from publicly available databases that TGFBR3L is enriched in the pituitary of all mammalian species investigated to date, including humans (*25*, *27*, *62*, *63*). Second, TGFBR3L appears to uniquely bind inhibin B among TGFβ family members. Although we only investigated three such ligands here, it is unlikely that others will bind strongly, if at all, given the specificity of inhibin B versus the highly related inhibin A. It could be informative to examine activin B binding; however, we did not observe altered activin B action in cells stably expressing TGFBR3L (fig. S14). Third, loss of TGFBR3L function produces a specific and restricted set of phenotypes. We have not observed physiological changes in KO mice beyond the predicted increases in FSH and the downstream effects thereof. Fourth, attenuating inhibin B action via TGFBR3L produces a preferable fertility outcome to antagonism of all inhibin action. That is, the relatively modest increase in FSH levels in *Tgfbr3l* KO females was sufficient to enhance ovarian folliculogenesis and litter size. In contrast, blocking all or most inhibin (A and B) action in *Tgfbr3l* and betaglycan dKOs led to very high FSH levels, ovarian overstimulation, and infertility. In light of these observations,

blocking inhibin B action via TGFBR3L may prove to be a viable new strategy to selectively increase endogenous FSH production as a means to treat infertility and hypogonadism.

MATERIALS AND METHODS

Single-cell and nuclei analyses

Murine scRNA-seq and snATAC-seq datasets and details of the analyses were previously published (*23*). Human snRNA-seq and snATAC-seq datasets and details of the analyses can be found in (*26*).

DNA constructs

pCMV6-Entry (PS100001), murine TGFBR3L-Myc-DDK (MR225940), and human TGFBR3L-Myc-DDK (RC231159) were purchased from OriGene Technologies (Rockville, MD, USA). Revised human TGFBR3L-Myc-DDK was made in-house by excising the 5′ end of the coding sequence from the OriGene construct using an Asi SI restriction site located in the pCMV6 backbone and an internal Xho I site in human TGFBR3L and replacing it with the revised [see the "5′ and 3′ RACE" section below] 5′ end (purchased from Twist Bioscience, San Francisco, CA, USA) using the same restriction sites.

The murine Myc-TGFBR3L-hemagglutinin (HA) construct was generated in two sequential rounds of cloning. First, the *Tgfbr3l* coding sequence (CDS) in the murine TGFBR3L-Myc-DDK plasmid was subcloned into a vector with a pcDNA3.1 backbone containing an N-terminal Myc tag preceded by a signal peptide to generate a murine Myc-TGFBR3L construct. Second, the CDS containing murine Myc-TGFBR3L was subcloned into a vector with a pcDNA3.0 backbone containing a C-terminal triple-HA tag to generate the final murine Myc-TGFBR3L-HA construct.

Rat betaglycan (TGFBR3) in pCMV5 with an N-terminal Myc tag was provided by T. Woodruff (Northwestern University, Chicago, IL, USA) and subcloned into pCMV6-Entry. The $CAGA_{12}$-luciferase and A3-luciferase reporters and the FAST2 can be replaced with forkhead box H1 (FAST1) plasmid were previously described (*55*, *64*, *65*). Expression plasmids for TGFβ2 and the $BG_{ZP\text{-}C}$ were previously described (*66*).

The murine TGFBR3L ECD (R36-R211; UniProt D3YZZ2) and human ActRII ECD (G23-T123; UniProt P27037) were amplified from synthetic double-stranded DNA fragments (Twist Bioscience, San Francisco, CA, USA) using primers that inserted a 5′ Not I restriction site and a 3′ Xho I restriction site. The TGFBR3L fragment coded for the region of the murine TGFBR3L ectodomain indicated above, followed by an Ile-Glu-Gly-Arg factor Xa cleavage site and a 3′ His6 tag. The ActRII fragment coded for a 5′ His6 tag, followed by a Ser-Ser-Gly linker, a Leu-Val-Pro-Arg-Gly-Ser thrombin cleavage site, and a His-Met dipeptide, followed by the coding sequence for the region of the human ActRII ectodomain indicated above. The TGFBR3L ECD-His6 and His6-ActRII ECD amplicons were inserted into a pcDNA3.1+ backbone (V79020, Invitrogen, Waltham, MA, USA) containing a rat serum albumin signal peptide 5′ to the Not I restriction site.

The mature human inhibin βA chain (G311-S426, UniProt P08476) was amplified from a synthetic double-stranded DNA fragment (Twist Bioscience) using primers that inserted 5′ Nde I and 3′ Hind III restriction sites. The amplicon was ligated into Novagen pET32a (69015-3, EMD Millipore, Burlington, MA, USA).

Human pituitary RNA

Human anterior pituitary glands were sampled and frozen at autopsy from accidental-death persons (aged 65 to 80 years) (*67*). Total RNA was extracted from frozen specimens using the mirVana miRNA Isolation Kit (AM1560, Invitrogen, Waltham, MA, USA) following the manufacturer's instructions. Ethics protocols were approved by the Institutional Review Board of the Faculty of Medicine of McGill University (Montreal, QC, CAN; A12-M117-11A and A08-M61-09B). Normal postnatal pituitary tissues were collected under the regulations of Cambridgeshire 1 Research Ethics Committee (Cambridge, UK; 06/Q0104/133).

5′ and 3′ RACE

5′ and 3′ RACE were performed using the FirstChoice RLM-RACE Kit (AM1700, Invitrogen) following the manufacturer's protocol. Briefly, intact 5′ capped mRNA in 10 μg of total adult human pituitary RNA was decapped and ligated to the 5′ RACE adaptor. The ligated mRNA was reverse-transcribed (as described below) using a gene-specific primer located in exon 3 (see table S2). Nested polymerase chain reaction (PCR) was performed on the resulting cDNA using adaptor-specific forward primers and gene-specific reverse primers located in exon 2 (see table S2). For 3′ RACE, 1 μg of total adult human pituitary RNA was reverse-transcribed using the 3′ RACE adaptor provided in the kit. Nested PCR was performed on the resulting cDNA using gene-specific forward primers located in exon 5 (see table S2) and adaptor-specific reverse primers. For both 5′ and 3′ RACE, PCR products were cloned into pGEM-T Easy (A1360, Promega, Madison, WI, USA) and sequenced (Génome Québec, Montreal, QC, CAN).

PCR amplification of *TGFBR3L*

To amplify the regions of the *TGFBR3L* CDS that were not determined by RACE, 1.5 μg of total adult human pituitary RNA was reverse-transcribed using random hexamers. The resulting cDNA was used to PCR-amplify segments of the CDS, spanning exon-exon junctions (see table S2). PCR amplicons were purified using the GenepHlow Gel/PCR Kit (DFH300, Geneaid, New Taipei City, Taiwan) and sequenced (Génome Québec).

Cell lines

All cells were cultured at 37°C in a humidified incubator with 5% CO_2. Human embryonic kidney (HEK) 293T cells [American Type Culture Collection (ATCC) CRL-3216; provided by T. Hébert, McGill University] and 293 cells (ATCC CRL-1573; provided by P. Branton, McGill University) were cultured in Dulbecco's modified Eagle's medium (DMEM) (319-005-CL, Wisent, St-Bruno, QC, Canada) supplemented with 5% (v/v) fetal bovine serum (FBS) (098150, Wisent). Immortalized murine gonadotrope-like LβT2 cells (*68*) (provided by P. Mellon, University of California, San Diego, CA, USA) were cultured in DMEM supplemented with 10% (v/v) FBS. CHO cells (ATCC CCL-61; provided by P. Morris, The Population Council, New York, NY, USA) were cultured in DMEM/F12 (319-075-CL, Wisent) supplemented with 10% (v/v) FBS. Expi293F cells were purchased from Invitrogen (A14527) and cultured in expi293 medium (A1435102, Invitrogen). The human granulosa tumor cell line, COV434, was cultured in DMEM supplemented with 10% (v/v) fetal calf serum.

To generate stable cell lines, CHO cells were seeded in a six-well plate at a density of 400,000 cells per well. Twenty-four hours later, cells were transfected with 1.5 μg of linearized pCMV6-Entry, revised human TGFBR3L-Myc-DDK, murine TGFBR3L-Myc-DDK, or rat Myc-TGFBR3 (all in pCMV6-Entry) per well using polyethylenimine

(PEI) at a concentration of 1:3 (DNA to PEI). The following day and every second day after that, cells were treated with G-418 sulfate solution (800 μg/ml; 450-130-QL, Wisent). After a week of treatment, surviving G-148–resistant cells were plated into 96-well plates at a density of 0.5 cell per well. Monoclonal colonies were expanded until there were sufficient cells to both freeze down and lyse for protein extraction. Following immunoblotting of protein lysates from the CHO stable clones (see the "Immunoblotting" section below), lines with the highest expression of the desired protein were used for promoter-reporter assays (see the "Promoter-reporter assays" section below).

Deglycosylation

For deglycosylation assays, HEK293T cells were seeded in a six-well plate at a density of 800,000 cells per well. The following day, cells were transfected with 2 μg of pCMV6-Entry, murine TGFBR3L-Myc-DDK, or human (OriGene or revised) TGFBR3L-Myc-DDK using PEI at a mass ratio of 1:3 (DNA to PEI). Twenty-four hours after transfection, cells were lysed in radioimmunoprecipitation assay (RIPA) buffer containing protease inhibitors and protein concentration measured using a Pierce BCA protein assay kit (23227, Thermo Fisher Scientific, Waltham, MA, USA) following the manufacturer's instructions. Forty micrograms of each protein lysate was denatured at 75°C for 15 min, cooled on ice for 10 min, deglycosylated with 500 U of Endo H (P0702, New England BioLabs, Whitby, ON, Canada) or 500 U of peptide *N*-glycosidase F (PNGase F) (P0704, New England BioLabs), or left untreated and incubated at 37°C for 2 hours before immunoblotting (see the "Immunoblotting" section below).

Cell surface biotinylation and immunoprecipitation

Two million HEK293 cells were seeded per 10-cm dish. Twenty-four hours later, cells were transfected with 7 μg of either pCMV6-Entry, murine TGFBR3L-Myc-DDK, or revised human TGFBR3L-Myc-DDK using PEI at a ratio of 1:3 (DNA to PEI). The following day, cells were washed with cold 1× phosphate-buffered saline (PBS) and incubated with 5 mg of EZ-Link Sulfo-NHS-LC-Biotin (21335, Thermo Fisher Scientific) diluted in 1× PBS for 15 min. Cells were then washed with 100 mM glycine in 1× PBS, lysed in buffer [50 mM tris-HCl (pH 7.4), 150 mM NaCl, 1 mM EDTA, and 1% Triton X-100], and cleared by centrifugation. Supernatant was collected, and immunoprecipitation was carried out using EZview Red Anti-FLAG M2 Affinity Gel (F2426, MilliporeSigma; RRID:AB_2616449) following the manufacturer's instructions. Twenty microliters of total and immunoprecipitated lysates were immunoblotted (see the "Immunoblotting" section below).

Immunoblotting

Cell lysates were denatured with Laemmli buffer [250 mM tris (pH 6.8), 10% SDS, 50% glycerol, 0.2% bromophenol blue, and 10% β-mercaptoethanol] at 75°C for 15 min and resolved by SDS-PAGE on a 10% resolving gel prepared using a 30% (w/w) acrylamide/bis-acrylamide (29:1) solution in running buffer [25 mM tris, 250 mM glycine, and 0.1% SDS (pH 8.3)]. Proteins were transferred to Protran nitrocellulose membranes (GE 10600001, MilliporeSigma) in Towbin buffer [25 mM tris, 192 mM glycine (pH 8.3), and 20% methanol], blocked with 5% milk (w/v) in tris-buffered saline (TBS) [150 mM NaCl and 10 mM tris (pH 8.0)] containing 0.05% (v/v) Tween-20 (TBST) and incubated overnight at 4°C with agitation with the indicated primary antibodies diluted in blocking buffer. For cell surface biotinylation following transfer, membranes were blocked with 5% bovine serum albumin (BSA) in TBST and incubated with a VECTASTAIN Elite ABC-HRP kit (PK6100, Vector Laboratories, Burlington, ON, Canada) as per the manufacturer's guidelines. The monoclonal mouse anti–c-Myc (1:1000; M5546, RRID:AB_260581), mouse anti–β-actin (1:40,000; A5441, RRID:AB_476744), and rabbit anti-FLAG (1:500; F7425, RRID:AB_439687) were purchased from MilliporeSigma. The monoclonal mouse anti–α-tubulin (1:10,000; ab7291, RRID:AB_2241126) was purchased from Abcam (Cambridge, UK). The following day, membranes were washed in TBST and incubated in horseradish peroxidase–conjugated anti-mouse or anti-rabbit secondary antibodies [1:5000, goat anti-mouse (1706516, RRID:AB_11125547) and goat anti-rabbit (1706515, RRID:AB_11125142, Bio-Rad Laboratories, Saint-Laurent, QC, Canada)] in blocking buffer for 1 hour at room temperature with agitation. Membranes were once again washed in TBST, enhanced chemiluminescence substrate (NEL105001, PerkinElmer, Waltham, MA, USA) was added, and bands were visualized with an Amersham Imager 600 (GE Healthcare, Chicago, IL, USA).

To compare the relative purities of inhibin B from R&D Systems (677-IB/CF, Minneapolis, MN, USA) and AnshLabs (AG-306-AI100, Webster, TX, USA), 20 ng of each sample was denatured under nonreducing conditions (10% β-mercaptoethanol omitted from Laemmli buffer) and resolved by SDS-PAGE on a 12% gel prepared using a 30% (w/w) acrylamide/bis-acrylamide (29:1) and immunoblotted, as described above. The monoclonal mouse anti-inhibin βB (1:3000; AB-306-AA042; RRID:AB_2756475) was purchased from AnshLabs.

To assess siRNA knockdown, 150,000 HEK293 cells per well were seeded in a six-well plate. The following day, cells were transfected with 300 ng per well of either pCMV6, murine TGFBR3L-Myc-DDK, or Myc-TGFBR3 in combination with 2 nM control siGENOME nontargeting (D-001210-05-05) or *Tgfbr3l* siGENOME SMARTpool (D-0169776) siRNA (both from Dharmacon, Lafayette, CO, USA) using Lipofectamine 3000 Transfection Reagent (3 μl per well; L3000015, Thermo Fisher Scientific). Two days after transfection, cells were lysed in RIPA buffer containing protease inhibitors and protein concentration measured using the Pierce BCA protein assay kit and immunoblotted as described above.

Immunofluorescence

Circular coverslips (12-545-81P, Thermo Fisher Scientific) were placed in 24-well plates and coated with 2.6× diluted Matrigel (356234, Corning Inc., Corning, NY, USA). Next, HEK293 cells were seeded at a density of 50,000 cells per well. The following day, cells were transfected with 400 ng per well of either pCMV6, murine Myc-TGFBR3L-HA, or human (revised) TGFBR3L-Myc-DDK using Lipofectamine 3000 Transfection Reagent (1.3 μl per well). Twenty-four hours after transfection, cells were fixed with 4% (w/v) paraformaldehyde (P6148, MillliporeSigma) for 15 min and washed with PBS. Where indicated, cells were permeabilized with PBS containing 0.5% (v/v) Triton X-100 for 15 min. In all conditions, cells were blocked for 1 hour with PBS containing 15% (v/v) goat serum (053-110, Wisent). Cells were incubated overnight at 4°C with the indicated primary antibody diluted in blocking solution. Primary antibody dilutions were as follows: monoclonal mouse anti–c-Myc (1:500), monoclonal mouse anti-HA (1:500; H9658, MilliporeSigma, RRID:AB_260092), and polyclonal rabbit anti-human TGFBR3L (1:50; NBP2-57581, Novus Biologicals, Centennial, CO, USA,

RRID:AB_2889137). The following day, cells were washed with PBS and then incubated with either goat anti-mouse Alexa Fluor 488 (A-21121, Thermo Fisher Scientific, RRID:AB_2535764) or donkey anti-rabbit Alexa Fluor 488 (A-21206, Thermo Fisher Scientific, RRID:AB_2535792) diluted 1:500 in blocking solution for 1 hour. Cells were washed with PBS, and coverslips were mounted on slides using Prolong Fold Antifade reagent with 4′,6-diamidino-2-phenylindole (DAPI) (1266174, Thermo Fisher Scientific). Confocal images were captured with a Leica SP8 LSM using a Leica HC PL CS2 63×/1.4 numerical aperture oil objective. The images were collected sequentially using a Leica HyD detector. Alexa 488 excitation was performed using a 488-nm optically pumped semiconductor lasers (OPSL) laser 20 mW at 2.6%, and DAPI excitation was performed using a Coherent Cameleon Vision 2 multiphoton laser, wavelength at 720 nM and power at 2.296 W (0.6%). Emission detection windows were set at 503 to 575 nm for Alexa Fluor 488 and 407 to 569 nm for DAPI.

Promoter-reporter assays

For promoter-reporter assays, CHO stable or LβT2 cells were seeded at densities of 30,000 or 150,000 cells per well, respectively, in 48-well plates. The following day, CHO cells were transfected with CAGA-luc (200 ng per well) using PEI at a ratio of 1:3 (DNA to PEI), and LβT2 cells were transfected with CAGA-luc (200 ng per well) and 2 nM of control siGENOME nontargeting, betaglycan siGENOME SMARTpool (D-046537, Dharmacon) or *Tgfbr3l* siGENOME SMARTpool siRNA using Lipofectamine 3000 Transfection Reagent (1 μl per well). For double knockdown experiments, either 4 nM control or 2 nM each of betaglycan and *Tgfbr3l* siRNA were used. Twenty-four hours after transfection, cells were serum-starved for an additional 24 hours. Following serum starvation, cells were treated with vehicle, 1 nM activin A (338-AC, R&D Systems), 0.01 to 5 nM activin B (659-AB, R&D Systems), and/or recombinant inhibin A (0.01, 0.1, or 1 nM; 624-IN, R&D Systems) or inhibin B [0.01, 0.1, 1, and 5 nM; AnshLabs or R&D Systems (fig. S15)] for 6 hours and then lysed in passive lysis buffer (50 μl per well) [25 mM tris-phosphate (pH 7.8), 10% (v/v) glycerol, 1% (v/v) Triton X-100, BSA (1 mg/ml), and 2 nM EDTA] for 20 min at room temperature with agitation. Twenty microliters of cell lysis supernatant was combined with 100 μl of assay buffer [final concentration: 15 nM potassium phosphate (pH 7.8), 25 nM glycylglycine, 15 mM magnesium sulfate, 4 nM EDTA, 2 nM adenosine 5′-triphosphate, 1 nM dithiothreitol, and 0.04 mM D-luciferin], and luciferase activity was measured on an Orion II microplate luminometer (Berthold Detection Systems, Oak Ridge, TN, USA). All conditions were performed in technical triplicates, and the experiments were repeated as indicated in the figure legends.

Promoter-reporter assays in COV434 cells were performed as previously described (*55*). Briefly, cells were plated in 48-well plates at a density of 75,000 cells per well. The following day, cells were transfected with A3-luc (50 ng per well), 100 ng of FAST1, and 50 ng of either pCMV6, Myc-betaglycan, or murine TGFBR3L-Myc-DDK using Lipofectamine 3000 according to the manufacturer's guidelines. Twenty-four hours after transfection, cells were treated with 200 pM activin A and the indicated amount of purified inhibin A or B [0, 0.02, 1, and 5 nM; as previously described (*55*)]. Twenty-four hours following treatment, cells were lysed in buffer [1% Triton X-100, 25 mM glycylglycine (pH 7.8), 15 mM $MgSO_4$, 4 mM EGTA, and 1 mM dithiothreitol] on ice for 10 min. Lysates were combined with an equal volume of VivoGlo Luciferin [Promega, WI, lysate (1 μg/50 μl)], and luciferase activity was measured using a CLARIOstar microplate reader (BMG Labtech, Germany).

SPR measurements

TGFβ2 E84A, a variant not shown to affect binding of TGFβ2 to rat betaglycan, was expressed in *Eschericha coli*, refolded, and purified as previously described (*29*). Activin A was expressed in *E. coli* in the form of insoluble inclusion bodies at 37°C. Isolation of the inclusion bodies, reconstitution, refolding, and purification were as previously described (*69*). Rat $BG_{ZP\text{-}C}$, the ECD of murine TGFBR3L, and His-ActRII ECD were expressed and purified from suspension cultured expi293F cells by immobilized metal affinity chromatography and size exclusion chromatography (*66*).

SPR datasets were generated using a BIAcore X100 instrument (Cytiva, Piscataway, NJ). Sensor surfaces were generated either by capturing carboxy-biotinylated Avi-tag ligand onto a neutravidin-coated CM5 sensor chip (Cytiva, Piscataway, NJ) to a density of 50 to 150 RU (response units) (TGFβ2 E84A) or by direct coupling to an unmodified CM5 sensor chip to a density of 2000 to 3000 RU (activin A, produced in-house, and inhibins A and B, R&D Systems). Neutravidin-coated sensor chips for capture of biotinylated Avi-tag ligands were made by activating the surface of a CM5 chip with EDC (1-ethyl-3-[3-dimethylaminopropyl]carbodiimide hydrochloride) and NHS (*N*-hydroxy succinimide), followed by injection of neutravidin (2 mg/ml; Pierce, Rockford, IL) in 10 mM sodium acetate at pH 4.0 until the surface density reached 10,000 to 12,000 RU. Unreacted sites were blocked with an equimolar mixture of arginine and agmatine (200 mM each) at pH 8.5. Direct immobilization onto the sensor chips was achieved by activating the surface of a CM5 chip with EDC and NHS, followed by injection of 1 μM ligand in 10 mM sodium acetate at pH 4.0 until the surface density reached the RU specified above. Unreacted sites were blocked with an equimolar mixture of arginine and agmatine (200 mM each) at pH 8.5.

Kinetic binding assays were performed with analytes serially diluted in 10 mM Hepes (pH 7.4), 150 mM NaCl, 3 mM EDTA, and 0.01% surfactant P20 (Pierce, Rockford, IL). Injection series were performed in an interleaved manner and, in most cases, with duplicate or triplicate injections at 100 μl/min. Regeneration of the surface was achieved with a 10-s injection of 200 mM guanidine hydrochloride, pH 2.0. Baseline correction was performed by subtracting the response both from the reference surface with no immobilized ligand and 5 to 10 blank buffer injections. Kinetic analyses were performed by fitting the results to a simple 1:1 model using the program Scrubber (Biologic Software, Canberra, Australia).

Animal housing

All mice were housed on a 12-hour lights on/12-hour lights off cycle and were given ad libitum access to food and water. All animals were anesthetized with isoflurane and euthanized by CO_2 asphyxiation. All animal work was conducted in accordance with federal and institutional guidelines and with the approval of the Facility Animal Care Committee (Downtown Campus A) at McGill University (protocol no. 5204).

Development of *Tgfbr3l*-deficient mice

Four gRNAs were designed to target introns on either side of *Tgfbr3l* exon 2 (see table S2). Mice were generated by electroporation of the four sgRNAs (Synthego) and Cas9 protein (1081059, Integrated DNA Technologies Inc., Coralville, IA, USA) into single-cell C57BL6/N

mouse zygotes (Strain 475, Charles River Laboratories, Senneville, QC, Canada). The electroporation was performed at the McGill Integrated Core for Animal Modelling at the Goodman Cancer Research Center Mouse Transgenic Facility of McGill University. The electroporated zygotes were cultured overnight in EmbryoMax Advanced KSOM Embryo Medium (MR-101-D, MilliporeSigma) droplets under mineral oil in a 35-mm dish at 37°C in a 5% CO_2 incubator. Embryos were transferred to the oviducts of pseudopregnant CD1-Elite females (Strain 482, Charles River Laboratories). Live pups born from these females were genotyped by PCR amplification of genomic DNA extracted from tail biopsies. The targeted region was amplified using two different sets of genotyping primers (see table S2), resolved on a 1% agarose gel, and gel-purified. The products were sent for direct Sanger sequencing (Génome Québec). A founder male had 200–base pair (bp) and 684-bp deletions in his two *Tgfbr3l* alleles. The 684-bp deletion included exon 2 and was germline transmissible. Therefore, this mutation was pursued (*Tgfbr3l*^{em2Djb}; MGI:6460397). Heterozygous *Tgfbr3l*$^{+/-}$ mice were crossed inter se to generate WT *Tgfbr3l*$^{+/+}$, heterozygous *Tgfbr3l*$^{+/-}$, and KO *Tgfbr3l*$^{-/-}$ animals.

Generation of *Tgfbr3* and *Tgfbr3l* dKO mice

The *Tgfbr3*$^{fl/fl}$ (*Tgfbr3*$^{tm1.1Hlin}$; MGI (Mouse Genome Informatics): 6220924) and *Gnrhr*$^{Cre/+}$ [GnRHR-IRES-Cre (GRIC); *Gnrhr*$^{tm1(cre)Uboe}$; MGI: 3795249] mice were previously described (*20*, *70*). *Gnrhr*$^{Cre/+}$;*Tgfbr3*$^{fl/fl}$ females (*20*) were crossed with *Tgfbr3l*$^{-/-}$ males to generate *Gnrhr*$^{Cre/+}$;*Tgfbr3*$^{+/fl}$;*Tgfbr3l*$^{+/-}$ females. These females were then crossed with *Gnrhr*$^{+/+}$;*Tgfbr3*$^{fl/fl}$ males to generate *Gnrhr*$^{Cre/+}$;*Tgfbr3*$^{fl/fl}$;*Tgfbr3l*$^{+/-}$ females and *Gnrhr*$^{+/+}$;*Tgfbr3*$^{+/fl}$;*Tgfbr3l*$^{+/-}$ males, which were crossed inter se. Their *Gnrhr*$^{Cre/+}$;*Tgfbr3*$^{fl/fl}$;*Tgfbr3l*$^{+/-}$ female and *Gnrhr*$^{+/+}$;*Tgfbr3*$^{fl/fl}$;*Tgfbr3l*$^{-/-}$ male progeny were intercrossed to generate *Gnrhr*$^{+/+}$;*Tgfbr3*$^{fl/fl}$;*Tgfbr3l*$^{+/-}$ (referred to as *Tgfbr3l*$^{+/-}$), *Gnrhr*$^{+/+}$;*Tgfbr3*$^{fl/fl}$;*Tgfbr3l*$^{-/-}$ (referred to as *Tgfbr3l*$^{-/-}$), and *Gnrhr*$^{Cre/+}$;*Tgfbr3*$^{fl/fl}$;*Tgfbr3l*$^{-/-}$ (dKO) animals. Genotyping was conducted using the primers listed in table S2.

Puberty onset, estrous cyclicity, and fertility assessment

Vaginal opening, an indicator of puberty onset, was monitored daily following weaning at postnatal day 21. Starting at 6 weeks of age, for a total of 3 weeks, estrous cyclicity was assessed daily by vaginal cytology using 0.1% methylene blue, following previously established guidelines (*71*). At 9 weeks of age, females were paired with WT C57BL/6 males (strain 027, Charles River Laboratories) for 3 to 6 months. Breeding cages were monitored daily to record litter frequency and size. Litters were euthanized at postnatal day 10.

Blood collection and hormone analysis

Blood collected from 9- to 13-week-old males or 9- to 10-week-old females by cardiac puncture was allowed to coagulate at room temperature for 30 min and spun down for 10 min at 800*g*. Serum was collected and stored at −20°C. Serum FSH and LH levels were assessed using in-house enzyme-linked immunosorbent assays (ELISAs) as previously described (detection ranges, 0.03125 to 0.5 ng/ml and 0.117 to 30 ng/ml, respectively) (*72*, *73*). Serum inhibins A (AL-161) and B (AL-163) were measured by ELISA (AnshLabs; detection ranges, 7.5 to 700 pg/ml and 6 to 1143 pg/ml, respectively). Serum progesterone was measured by ELISA (IB79105, Immuno-Biological Laboratories Inc., Minneapolis, MN, USA; detection range, 0.3 to 40 ng/ml).

Organ collection and processing

To assess *Tgfbr3l* expression in different tissues, pituitary glands, ovaries, testes, adrenals, brain, liver, kidneys, heart, lungs, stomach, intestine, colon, fat, femora, epididymides, uteri, and prostates were dissected from 8-week-old C57BL/6 males or females. Tissues were snap-frozen in liquid nitrogen and stored at −80°C. RNA was extracted from organs as described below.

Testes, epididymides, and seminal vesicles were dissected from 9- to 13-week-old males. Organs were weighed on an analytical balance. One testis per male was immersed in Bouin's Fixative Solution (1120-16, Ricca Chemical Company, Arlington, TX, USA) overnight at room temperature, followed by a 24-hour incubation in 100% ethanol. Testes were stored in 70% ethanol. Two fixed testes from each genotype were paraffin-embedded, sectioned, and stained with hematoxylin/eosin at the McGill Centre for Bone and Periodontal Research.

Pituitary glands, ovaries, and uteri were dissected from 9- to 10-week-old females on the morning of diestrus (~10:00). Pituitary glands and one ovary were snap-frozen in liquid nitrogen and stored at −80°C. One ovary and the uterus were weighed on an analytical balance. The ovary was then fixed in 10% neutral buffered formalin (HT501128, MilliporeSigma) overnight at room temperature and then stored in 70% ethanol. Fixed ovaries were paraffin-embedded, sectioned, and stained with hematoxylin/eosin at the McGill Centre for Bone and Periodontal Research.

All hematoxylin/eosin images were acquired with a Leica Microsystems DFC310 FC1.4-megapixel digital color camera on a Leica Microsystems DM1000 light-emitting diode microscope. Follicle counting by two investigators blinded to genotype was done on fully cut-through ovaries.

For pituitary FSH content, snap-frozen pituitaries were homogenized in 600 µl of PBS for 10 s using a Polytron (PT 10/35, Kinematica) and cleared by centrifugation, and the supernatant was diluted 1:100 in PBS before measuring FSH by ELISA (see the "Blood collection and hormone analysis" section above).

RNAscope mRNA in situ hybridization

Pituitaries were dissected from 8-week-old WT and KO males and fixed in 10% neutral buffered formalin for 18 hours at room temperature with rotation. Pituitaries were washed three times in PBS for 1 hour at room temperature and then dehydrated through a series of washes in 25, 50, 70, and 70% ethanol for 1 hour each. Pituitaries were paraffin-embedded and sectioned to a 5-micron thickness. Comparable sections from both genotypes were mounted together on Superfrost Plus slides (10149870, Fisher Scientific). Slides were pretreated according to the manufacturer's recommendations [322452, Advanced Cell Diagnostics (ACD), Newark, CA, USA] with the following conditions: slides were baked at 60°C for 1 hour on the morning of the first day, dewaxed twice for 5 min in xylenes, washed twice for 1 min in 100% EtOH, and then air-dried. ImmEdge Hydrophobic Barrier PAP pen (H-4000, Vector, Burlingame, CA, USA) was used to demarcate the area around adjacent sections. Pretreatment 2 solution was warmed to and maintained at 98°C in a glass beaker using a hot plate. Slides were immersed for 12 min in pretreatment 2 solution, followed by 30 min in pretreatment 3 solution at 40°C in a HybEZ oven (ACD). Specific probes against *Tgfbr3l* (custom-designed, ACD), along with *Ppib* (positive control, 313911, ACD), and *DapB* (negative control, 310043, ACD) were hybridized for 2 hours at 40°C in the HybEZ oven. Slides were

stored in 5× SSC overnight at room temperature. Single-plex RED RNAscope (322360, ACD) was continued as per the manufacturer's recommendations the following day. Hematoxylin QS (H-3404, Vector) was used as a nuclear counterstain. Slides were scanned using a Nanozoomer-XR Digital Slide Scanner (Hamamatsu) and processed using a Nanozoomer Digital Pathology View (Hamamatsu).

Natural ovulation

Eight- to nine-week-old females were mated with WT C57BL/6 males. On the morning of vaginal plug, females were euthanized, and the cumulus-oocyte complexes (COCs) were harvested from the ampullae of both oviducts. COCs were digested with hyaluronidase (0.5 mg/ml; H3884, MilliporeSigma) for 5 to 10 min at room temperature until dissociated. The number of oocytes was counted using an inverted microscope.

Superovulation

Twenty-five– to 30-day-old females were intraperitoneally injected with 5 IU pregnant mare serum gonadotropin (HOR-272, Prospec-Tany TechnoGene Ltd., East Brunswick, NJ, USA) between 16:00 and 17:00. Two days later, females were intraperitoneally injected with 5 IU human chorionic gonadotropin (C1063, MilliporeSigma) between 17:00 and 18:00. The following morning, females were euthanized, COCs were harvested, and the oocytes were counted as described for natural ovulation.

AIS preparation and injection

Lyophilized AIS (*74*) (Central Research, Tokyo, Japan) was dissolved in sterile H_2O to a concentration of 1 g/ml and stored at −80°C. On the morning of diestrus (07:00), females were intraperitoneally injected with 100 mg of AIS. Blood was collected by submandibular venipuncture before and 11 hours after the injection. Serum was extracted and stored at −20°C until the FSH ELISA.

Uterine implantation site assessment

Eight- to nine-week-old females were mated with WT C57BL/6 males. The morning of vaginal plug was considered 0.5 day post coitus (dpc). At 07:00 on 5.5 dpc, females were intravenously injected with 100 µl of 1% Evans blue dye (E2129, MilliporeSigma, dissolved in saline). Five minutes after injection, females were euthanized, uteri were dissected, and implantation sites were counted.

Primary pituitary cultures and inhibin treatment

Primary pituitary cultures were performed as previously described (*75*). Eight- to 14-week-old males were euthanized as described above, and their pituitaries were placed in M199 medium (M7653, MilliporeSigma) supplemented with 10% (v/v) FBS. Pituitaries were washed three times in Hank's balanced salt solution (HBSS) (311-511-CL, Wisent), chopped using a scalpel blade, and digested in collagenase [1.5 mg/ml; C-0130, MilliporeSigma, diluted in HBSS with bovine serum albumin (30 mg/ml, pH7.4); 40 µl per pituitary] for 2 hours at 37°C with gentle stirring. The digested pituitaries were then washed with calcium-free HBSS, centrifuged for 5 min at 1200*g*, and resuspended in pancreatin solution (P3292; Sigma-Aldrich; 4.5 mg/ml in calcium-free HBSS; 40 µl per pituitary). Pituitaries were digested in pancreatin for 7 min in a 37°C water bath with manual agitation. The cell suspension was then washed three times with M199 medium supplemented with 10% (v/v) FBS, with centrifugation in between steps, and cells were seeded in a 48-well plate at a density of 300,000 cells per well. The following morning, cells were treated with recombinant inhibin A (0.01, 0.1, or 1 nM) or inhibin B (0.01, 0.1, or 1 nM, AnshLabs) diluted in M199 medium supplemented with 2% (v/v) FBS. Twenty-four hours following treatment, RNA was extracted [see the "RNA extraction and reverse transcription quantitative PCR" section below].

RNA extraction and reverse transcription quantitative PCR

RNA was extracted from tissues and LβT2 cells using TRIzol reagent (15596018, Invitrogen, Waltham, MA, USA) following the manufacturer's protocol. For primary pituitary cultures, RNA was extracted using the Total RNA Mini Kit (FA32808-PS, Geneaid) following the manufacturer's protocol. For the assessment of *Tgfbr3l* expression in different tissues and in LβT2 cells, 1 µg of total RNA was reverse-transcribed. For all other experiments, 200 ng (tissue) or 100 ng (primary culture) of total RNA was reverse-transcribed.

RNA was reverse-transcribed using random hexamers (C1181, Promega) and Moloney murine leukemia virus reverse transcriptase (M1701, Promega). The resulting cDNA was used for qPCR analysis using EvaGreen (ABMMmix, Diamed, Missisauga, ON, Canada) and primers listed in table S2 on a Corbett Rotorgene 600 instrument (Corbett Life Science, Sydney, NSW, Australia). mRNA levels were determined using the $2^{-\Delta\Delta CT}$ method. Gene expression was normalized to ribosomal protein L19 (*Rpl19*). All primers were validated for efficiency and specificity.

Statistical analyses

Luciferase assay data from CHO and COV434 cells were analyzed by two-way analysis of variance (ANOVA), followed by Tukey's multiple comparisons test. siRNA knockdown luciferase assays and pituitary culture data were analyzed by two-way ANOVA, followed by Sidak's multiple comparisons test. Where indicated, effects of genotype between two groups were assessed by unpaired *t* test with Welch's correction. Effects of genotype between three groups were assessed by Brown-Forsythe and Welch's one-way ANOVA, followed by Dunnett's T3 multiple comparisons test. Statistical analyses were performed using Prism 9, GraphPad software. $P < 0.05$ was considered statistically significant.

SUPPLEMENTARY MATERIALS

Supplementary material for this article is available at https://science.org/doi/10.1126/sciadv.abl4391

View/request a protocol for this paper from *Bio-protocol*.

REFERENCES AND NOTES

1. A. P. N. Themmen, I. T. Huhtaniemi, Mutations of gonadotropins and gonadotropin receptors: Elucidating the physiology and pathophysiology of pituitary-gonadal function. *Endocr. Rev.* **21**, 551–583 (2000).
2. B. Lunenfeld, W. Bilger, S. Longobardi, V. Alam, T. D'Hooghe, S. K. Sunkara, The development of gonadotropins for clinical use in the treatment of infertility. *Front. Endocrinol.* **10**, 429 (2019).
3. D. J. Bernard, C. L. Smith, E. Brule, A tale of two proteins: βglycan, IGSF1, and the continuing search for the inhibin B receptor. *Trends Endocrinol. Metab.* **31**, 37–45 (2020).
4. Y. Makanji, J. Zhu, R. Mishra, C. Holmquist, W. P. S. Wong, N. B. Schwartz, K. E. Mayo, T. K. Woodruff, Inhibin at 90: From discovery to clinical application, a historical review. *Endocr. Rev.* **35**, 747–794 (2014).
5. A. J. Mason, J. S. Hayflick, N. Ling, F. Esch, N. Ueno, S. Y. Ying, R. Guillemin, H. Niall, P. H. Seeburg, Complementary DNA sequences of ovarian follicular fluid inhibin show precursor structure and homology with transforming growth factor-β. *Nature* **318**, 659–663 (1985).
6. F. H. de Jong, A. J. Grootenhuis, I. A. Klaij, W. M. Van Beurden, Inhibin and related proteins: Localization, regulation, and effects. *Adv. Exp. Med. Biol.* **274**, 271–293 (1990).

7. K. A. Lewis, P. C. Gray, A. L. Blount, L. A. MacConell, E. Wiater, L. M. Bilezikjian, W. Vale, Bglycan binds inhibin and can mediate functional antagonism of activin signalling. *Nature* **404**, 411–414 (2000).
8. J. W. Martens, J. P. de Winter, M. A. Timmerman, A. Mc Luskey, R. H. van Schaik, A. P. Themmen, F. H. de Jong, Inhibin interferes with activin signaling at the level of the activin receptor complex in Chinese hamster ovary cells. *Endocrinology* **138**, 2928–2936 (1997).
9. W. Vale, E. Wiater, P. Gray, C. Harrison, L. Bilezikjian, S. Choe, Activins and inhibins and their signaling. *Ann. N. Y. Acad. Sci.* **1038**, 142–147 (2004).
10. K. L. Walton, Y. Makanji, C. A. Harrison, New insights into the mechanisms of activin action and inhibition. *Mol. Cell. Endocrinol.* **359**, 2–12 (2012).
11. N. Ling, S. Y. Ying, N. Ueno, S. Shimasaki, F. Esch, M. Hotta, R. Guillemin, Pituitary FSH is released by a heterodimer of the β-subunits from the two forms of inhibin. *Nature* **321**, 779–782 (1986).
12. N. Ling, S. Y. Ying, N. Ueno, S. Shimasaki, F. Esch, M. Hotta, R. Guillemin, A homodimer of the β-subunits of inhibin A stimulates the secretion of pituitary follicle stimulating hormone. *Biochem. Biophys. Res. Commun.* **138**, 1129–1137 (1986).
13. W. Vale, J. Rivier, J. Vaughan, R. McClintock, A. Corrigan, W. Woo, D. Karr, J. Spiess, Purification and characterization of an FSH releasing protein from porcine ovarian follicular fluid. *Nature* **321**, 776–779 (1986).
14. B. Schmierer, C. S. Hill, TGFβ-SMAD signal transduction: Molecular specificity and functional flexibility. *Nat. Rev. Mol. Cell Biol.* **8**, 970–982 (2007).
15. J. Fortin, L. Ongaro, Y. Li, S. Tran, P. Lamba, Y. Wang, X. Zhou, D. J. Bernard, Minireview: Activin signaling in gonadotropes: What does the FOX say... to the SMAD? *Mol. Endocrinol.* **29**, 963–977 (2015).
16. Y. Li, G. Schang, U. Boehm, C. X. Deng, J. Graff, D. J. Bernard, SMAD3 regulates follicle-stimulating hormone synthesis by pituitary gonadotrope cells in Vivo. *J. Biol. Chem.* **292**, 2301–2314 (2017).
17. S. Tran, P. Lamba, Y. Wang, D. J. Bernard, SMADs and FOXL2 synergistically regulate murine FSHβ transcription via a conserved proximal promoter element. *Mol. Endocrinol.* **25**, 1170–1183 (2011).
18. S. C. Chapman, D. J. Bernard, J. Jelen, T. K. Woodruff, Properties of inhibin binding to βglycan, InhBP/p120 and the activin type II receptors. *Mol. Cell. Endocrinol.* **196**, 79–93 (2002).
19. J. Xu, K. McKeehan, K. Matsuzaki, W. L. McKeehan, Inhibin antagonizes inhibition of liver cell growth by activin by a dominant-negative mechanism. *J. Biol. Chem.* **270**, 6308–6313 (1995).
20. Y. Li, J. Fortin, L. Ongaro, X. Zhou, U. Boehm, A. Schneyer, D. J. Bernard, H. Y. Lin, Bglycan (TGFBR3) functions as an inhibin A, but not inhibin B, coreceptor in pituitary gonadotrope cells in mice. *Endocrinology* **159**, 4077–4091 (2018).
21. L. Y. M. Cheung, A. S. George, S. R. McGee, A. Z. Daly, M. L. Brinkmeier, B. S. Ellsworth, S. A. Camper, Single-cell RNA sequencing reveals novel markers of male pituitary stem cells and hormone-producing cell types. *Endocrinology* **159**, 3910–3924 (2018).
22. S. Qiao, K. Nordström, L. Muijs, G. Gasparoni, S. Tierling, E. Krause, J. Walter, U. Boehm, Molecular plasticity of male and female murine gonadotropes revealed by mRNA sequencing. *Endocrinology* **157**, 1082–1093 (2016).
23. F. Ruf-Zamojski, Z. Zhang, M. Zamojski, G. R. Smith, N. Mendelev, H. Liu, G. Nudelman, M. Moriwaki, H. Pincas, R. G. Castanon, V. D. Nair, N. Seenarine, M. A. S. Amper, X. Zhou, L. Ongaro, C. Toufaily, G. Schang, J. R. Nery, A. Bartlett, A. Aldridge, N. Jain, G. V. Childs, O. G. Troyanskaya, J. R. Ecker, J. L. Turgeon, C. K. Welt, D. J. Bernard, S. C. Sealfon, Single nucleus multi-omics regulatory landscape of the murine pituitary. *Nat. Commun.* **12**, 2677 (2021).
24. P. A. Fletcher, K. Smiljanic, R. Maso Prévide, J. R. Iben, T. Li, M. B. Rokic, A. Sherman, S. L. Coon, S. S. Stojilkovic, Cell type- and sex-dependent transcriptome profiles of rat anterior pituitary cells. *Front. Endocrinol.* **10**, 623 (2019).
25. E. Sjöstedt, A. J. Kolnes, N. C. Olarescu, N. Mitsios, F. Hikmet, Å. Sivertsson, C. Lindskog, K. A. B. Øystese, A. P. Jørgensen, J. Bollerslev, O. Casar-Borota, TGFBR3L—An uncharacterised pituitary specific membrane protein detected in the gonadotroph cells in non-neoplastic and tumour tissue. *Cancers* **13**, 114 (2021).
26. Z. Zhang, M. Zamojski, G. R. Smith, T. L. Willis, V. Yianni, N. Mendelev, H. Pincas, N. Seenarine, M. A. Amper, M. Vasoya, V. Nair, J. Turgeon, D. Bernard, O. Troyanskaya, C. Andoniadou, S. Sealfon, F. Ruf-Zamojski, Single nucleus pituitary transcriptomic and epigenetic landscape reveals human stem cell heterogeneity with diverse regulatory mechanisms. *bioRxiv*, 2021.2006.2018.449034 (2021).
27. T. Human Protein Atlas (2021); www.proteinatlas.org/ENSG00000260001-TGFBR3L/tissue.
28. E. Wiater, C. A. Harrison, K. A. Lewis, P. C. Gray, W. W. Vale, Identification of distinct inhibin and transforming growth factor β-binding sites on βglycan. *J. Biol. Chem.* **281**, 17011–17022 (2006).
29. M. A. Henen, P. Mahlawat, C. Zwieb, R. B. Kodali, C. S. Hinck, R. D. Hanna, T. C. Krzysiak, U. Ilangovan, K. E. Cano, G. Hinck, M. Vonberg, M. McCabe, A. P. Hinck, TGF-β2 uses the concave surface of its extended finger region to bind βglycan's ZP domain via three residues specific to TGF-β and inhibin-α. *J. Biol. Chem.* **294**, 3065–3080 (2019).
30. Y. Makanji, P. D. Temple-Smith, K. L. Walton, C. A. Harrison, D. M. Robertson, Inhibin B is a more potent suppressor of rat follicle-stimulating hormone release than inhibin a in vitro and in vivo. *Endocrinology* **150**, 4784–4793 (2009).
31. P. J. Illingworth, N. P. Groome, W. Byrd, W. E. Rainey, A. McNeilly, J. P. Mather, W. J. Bremner, Inhibin-B: A likely candidate for the physiologically important form of inhibin in men. *J. Clin. Endocrinol. Metab.* **81**, 1321–1325 (1996).
32. B. D. Anawalt, R. A. Bebb, A. M. Matsumoto, N. P. Groome, P. J. Illingworth, A. McNeilly, W. J. Bremner, Serum inhibin B levels reflect Sertoli cell function in normal men and men with testicular dysfunction. *J. Clin. Endocrinol. Metab.* **81**, 3341–3345 (1996).
33. T. M. Plant, V. Padmanabhan, S. Ramaswamy, D. McConnell, S. J. Winters, N. Groome, A. R. Midgley Jr., A. McNeilly, Circulating concentrations of dimeric inhibin A and B in the male rhesus monkey (*Macaca mulatta*). *J. Clin. Endocrinol. Metab.* **82**, 2617–2621 (1997).
34. S. Ramaswamy, G. R. Marshall, A. S. McNeilly, T. M. Plant, Dynamics of the follicle-stimulating hormone (FSH)-inhibin B feedback loop and its role in regulating spermatogenesis in the adult male rhesus monkey (*Macaca mulatta*) as revealed by unilateral orchidectomy. *Endocrinology* **141**, 18–27 (2000).
35. J. G. Pierce, T. F. Parsons, Glycoprotein hormones: Structure and function. *Annu. Rev. Biochem.* **50**, 465–495 (1981).
36. N. B. Schwartz, C. P. Channing, Evidence for ovarian "inhibin": Suppression of the secondary rise in serum follicle stimulating hormone levels in proestrous rats by injection of porcine follicular fluid. *Proc. Natl. Acad. Sci. U.S.A.* **74**, 5721–5724 (1977).
37. K. L. Stenvers, M. L. Tursky, K. W. Harder, N. Kountouri, S. Amatayakul-Chantler, D. Grail, C. Small, R. A. Weinberg, A. M. Sizeland, H. J. Zhu, Heart and liver defects and reduced transforming growth factor β2 sensitivity in transforming growth factor β type III receptor-deficient embryos. *Mol. Cell. Biol.* **23**, 4371–4385 (2003).
38. E. Wiater, K. A. Lewis, C. Donaldson, J. Vaughan, L. Bilezikjian, W. Vale, Endogenous βglycan is essential for high-potency inhibin antagonism in gonadotropes. *Mol. Endocrinol.* **23**, 1033–1042 (2009).
39. L. B. Draper, M. M. Matzuk, V. J. Roberts, E. Cox, J. Weiss, J. P. Mather, T. K. Woodruff, Identification of an inhibin receptor in gonadal tumors from inhibin α-Subunit knockout mice. *J. Biol. Chem.* **273**, 398–403 (1998).
40. P. G. Farnworth, C. A. Harrison, P. Leembruggen, K. L. Chan, P. G. Stanton, G. T. Ooi, N. A. Rahman, I. T. Huhtaniemi, J. K. Findlay, D. M. Robertson, Inhibin binding sites and proteins in pituitary, gonadal, adrenal and bone cells. *Mol. Cell. Endocrinol.* **180**, 63–71 (2001).
41. C. A. Harrison, P. G. Farnworth, K. L. Chan, P. G. Stanton, G. T. Ooi, J. K. Findlay, D. M. Robertson, Identification of specific inhibin A-binding proteins on mouse Leydig (TM3) and sertoli (TM4) cell lines. *Endocrinology* **142**, 1393–1402 (2001).
42. A. S. McNeilly, C. J. H. Souza, D. T. Baird, I. A. Swanston, J. Mc Verry, J. Crawford, M. Cranfield, G. A. Lincoln, Production of inhibin A not B in rams: Changes in plasma inhibin A during testis growth, and expression of inhibin/activin subunit mRNA and protein in adult testis. *Reproduction* **123**, 827–835 (2002).
43. A. E. O'Connor, D. M. De Kretser, Inhibins in normal male physiology. *Semin. Reprod. Med.* **22**, 177–185 (2004).
44. T. K. Woodruff, L. M. Besecke, N. Groome, L. B. Draper, N. B. Schwartz, J. Weiss, Inhibin A and inhibin B are inversely correlated to follicle-stimulating hormone, yet are discordant during the follicular phase of the rat estrous cycle, and inhibin A is expressed in a sexually dimorphic manner. *Endocrinology* **137**, 5463–5467 (1996).
45. C. K. Welt, Y. L. Pagan, P. C. Smith, K. B. Rado, J. E. Hall, Control of follicle-stimulating hormone by estradiol and the inhibins: Critical role of estradiol at the hypothalamus during the luteal-follicular transition. *J. Clin. Endocrinol. Metab.* **88**, 1766–1771 (2003).
46. Y. Makanji, C. A. Harrison, P. G. Stanton, R. Krishna, D. M. Robertson, Inhibin A and B in vitro bioactivities are modified by their degree of glycosylation and their affinities to βglycan. *Endocrinology* **148**, 2309–2316 (2007).
47. F. Lopez-Casillas, J. L. Wrana, J. Massague, Bglycan presents ligand to the TGF β signaling receptor. *Cell* **73**, 1435–1444 (1993).
48. G. De Crescenzo, C. S. Hinck, Z. Shu, J. Zúñiga, J. Yang, Y. Tang, J. Baardsnes, V. Mendoza, L. Z. Sun, F. López-Casillas, M. O'Connor-Mc Court, A. P. Hinck, Three key residues underlie the differential affinity of the TGFβ isoforms for the TGFβ type II receptor. *J. Mol. Biol.* **355**, 47–62 (2006).
49. J. Baardsnes, C. S. Hinck, A. P. Hinck, M. D. O'Connor-McCourt, TβR-II discriminates the high- and low-affinity TGF-β isoforms via two hydrogen-bonded ion pairs. *Biochemistry* **48**, 2146–2155 (2009).
50. A. J. Gore, D. P. Philips, W. L. Miller, D. J. Bernard, Differential regulation of follicle stimulating hormone by activin A and TGFB1 in murine gonadotropes. *Reprod. Biol. Endocrinol.* **3**, 73 (2005).
51. M. I. Suszko, T. K. Woodruff, Cell-specificity of transforming growth factor-β response is dictated by receptor bioavailability. *J. Mol. Endocrinol.* **36**, 591–600 (2006).

52. P. G. Farnworth, Y. Wang, R. Escalona, P. Leembruggen, G. T. Ooi, J. K. Findlay, Transforming growth factor-β blocks inhibin binding to different target cell types in a context-dependent manner through dual mechanisms involving βglycan. *Endocrinology* **148**, 5355–5368 (2007).
53. B. D. Looyenga, E. Wiater, W. Vale, G. D. Hammer, Inhibin-A antagonizes TGFβ2 signaling by down-regulating cell surface expression of the TGFβ coreceptor βglycan. *Mol. Endocrinol.* **24**, 608–620 (2010).
54. Y. Makanji, K. L. Walton, M. C. Wilce, K. L. Chan, D. M. Robertson, C. A. Harrison, Suppression of inhibin A biological activity by alterations in the binding site for βglycan. *J. Biol. Chem.* **283**, 16743–16751 (2008).
55. M. P. Goney, M. C. J. Wilce, J. A. Wilce, W. A. Stocker, G. M. Goodchild, K. L. Chan, C. A. Harrison, K. L. Walton, Engineering the ovarian hormones inhibin A and inhibin B to enhance synthesis and activity. *Endocrinology* **161**, bqaa099 (2020).
56. J. Esparza-Lopez, J. L. Montiel, M. M. Vilchis-Landeros, T. Okadome, K. Miyazono, F. López-Casillas, Ligand binding and functional properties of βglycan, a co-receptor of the transforming growth factor-β superfamily. Specialized binding regions for transforming growth factor-β and inhibin A. *J. Biol. Chem.* **276**, 14588–14596 (2001).
57. W. Sebald, T. D. Mueller, The interaction of BMP-7 and ActRII implicates a new mode of receptor assembly. *Trends Biochem. Sci.* **28**, 518–521 (2003).
58. L. S. Mathews, W. W. Vale, Expression cloning of an activin receptor, a predicted transmembrane serine kinase. *Cell* **65**, 973–982 (1991).
59. J. Greenwald, M. E. Vega, G. P. Allendorph, W. H. Fischer, W. Vale, S. Choe, A flexible activin explains the membrane-dependent cooperative assembly of TGF-β family receptors. *Mol. Cell* **15**, 485–489 (2004).
60. T. B. Thompson, T. K. Woodruff, T. S. Jardetzky, Structures of an ActRIIB:activin A complex reveal a novel binding mode for TGF-β ligand:receptor interactions. *EMBO J.* **22**, 1555–1566 (2003).
61. C. A. Harrison, P. C. Gray, W. H. Fischer, C. Donaldson, S. Choe, W. Vale, An activin mutant with disrupted ALK4 binding blocks signaling via type II receptors. *J. Biol. Chem.* **279**, 28036–28044 (2004).
62. The Tabula Muris Consortium; Overall coordination; Logistical coordination; Organ collection and processing; Library preparation and sequencing; Computational data analysis; Cell type annotation; Writing group; Supplemental text writing group and principal investigators, Single-cell transcriptomics of 20 mouse organs creates a Tabula Muris. *Nature* **562**, 367–372 (2018).
63. Tabula Muris Consortium, A single-cell transcriptomic atlas characterizes ageing tissues in the mouse. *Nature* **583**, 590–595 (2020).
64. S. Dennler, S. Itoh, D. Vivien, P. ten Dijke, S. Huet, J. M. Gauthier, Direct binding of Smad3 and Smad4 to critical TGF β-inducible elements in the promoter of human plasminogen activator inhibitor-type 1 gene. *EMBO J.* **17**, 3091–3100 (1998).
65. H. C. Huang, L. C. Murtaugh, P. D. Vize, M. Whitman, Identification of a potential regulator of early transcriptional responses to mesoderm inducers in the frog embryo. *EMBO J.* **14**, 5965–5973 (1995).
66. S. K. Kim, M. J. Whitley, T. C. Krzysiak, C. S. Hinck, A. B. Taylor, C. Zwieb, C.-H. Byeon, X. Zhou, V. Mendoza, F. López-Casillas, W. Furey, A. P. Hinck, Structural adaption in its orphan domain engenders βglycan with an alternate mode of growth factor binding relative to endoglin. *Structure* **27**, 1427–1442.e4 (2019).
67. J. Nadaf, L. de Kock, A. S. Chong, M. Korbonits, P. Thorner, N. Benlimame, L. Fu, A. Peet, J. Warner, O. Ploner, S. Shuangshoti, S. Albrecht, N. Hamel, J. R. Priest, B. Rivera, J. Ragoussis, W. D. Foulkes, Molecular characterization of DICER1-mutated pituitary blastoma. *Acta Neuropathol.* **141**, 929–944 (2021).
68. E. T. Alarid, J. J. Windle, D. B. Whyte, P. L. Mellon, Immortalization of pituitary cells at discrete stages of development by directed oncogenesis in transgenic mice. *Development* **122**, 3319–3329 (1996).
69. D. Ejima, K. Ono, K. Tsumoto, T. Arakawa, Y. Eto, A novel "reverse screening" to identify refolding additives for activin-A. *Protein Expr. Purif.* **47**, 45–51 (2006).
70. S. Wen, J.. R. Schwarz, D. Niculescu, C. Dinu, C. K. Bauer, W. Hirdes, U. Boehm, Functional characterization of genetically labeled gonadotropes. *Endocrinology* **149**, 2701–2711 (2008).
71. S. L. Byers, M. V. Wiles, S. L. Dunn, R. A. Taft, Mouse estrous cycle identification tool and images. *PLOS ONE* **7**, e35538 (2012).
72. L. Ongaro, C. A. I. Alonso, X. Zhou, E. Brûlé, Y. Li, G. Schang, A. F. Parlow, F. Steyn, D. J. Bernard, Development of a highly sensitive ELISA for measurement of FSH in serum, plasma, and whole blood in mice. *Endocrinology* **162**, bqab014 (2021).
73. F. J. Steyn, Y. Wan, J. Clarkson, J. D. Veldhuis, A. E. Herbison, C. Chen, Development of a methodology for and assessment of pulsatile luteinizing hormone secretion in juvenile and adult male mice. *Endocrinology* **154**, 4939–4945 (2013).
74. H. Wang, C. B. Herath, G. Xia, G. Watanabe, K. Taya, Superovulation, fertilization and in vitro embryo development in mice after administration of an inhibin-neutralizing antiserum. *Reproduction* **122**, 809–816 (2001).
75. L. Ongaro, X. Zhou, Y. Cui, U. Boehm, D. J. Bernard, Gonadotrope-specific deletion of the BMP type 2 receptor does not affect reproductive physiology in mice. *Biol. Reprod.* **102**, 639–646 (2020).

Acknowledgments: We would like to thank L. de Kock (McGill University), W. Foulkes (McGill University), and M. Korbonits (Queen Mary University of London) for providing the human pituitary RNA samples. T. Woodruff (Northwestern University) provided the rat betaglycan plasmid. T. Hébert (HEK293T, McGill University), P. Branton (HEK293, McGill University), P. Mellon (LβT2, University of California, San Diego), and P. Morris (CHO, The Population Council) provided immortalized cell lines. H. Y. Lin (Massachusetts General Hospital and Harvard Medical School) provided the floxed betaglycan mice. N. Audet from the Imaging and Molecular Biology Platform in the Department of Pharmacology and Therapeutics at McGill University facilitated the confocal imaging. **Funding:** This work was supported by Canadian Institutes of Health Research project grant PJT-162343 (to D.J.B.), NIH grant GM58670 (to A.P.H.), NIH grant DK46943 (to S.C.S.), Medical Research Council MR/T012153/1 (to C.L.A.), Natural Sciences and Engineering Research Council of Canada Doctoral Graduate Scholarship (to E.B.), Canadian Institutes of Health Research Master's Graduate Scholarship (to Y.-F.L.), and McGill University James Frosst Award (to Y.-F.L.). **Author contributions:** Conceptualization: E.B., A.P.H., and D.J.B. Investigation: E.B., Y.W., Y.L., Y.-F.L., X.Z., L.O., C.A.I.A., E.R.S.B., C.-H.B., C.S.H., A.P.H., N.M., F.R.-Z., J.P.R., K.L.W., and M.C. Formal analysis: E.B. and M.Z. Resources: A.L.S. and U.B. Supervision: S.C.S., C.L.A., C.A.H., A.P.H., and D.J.B. Writing—original draft: E.B., A.P.H., and D.J.B. Writing—review and editing: All authors. **Competing interests:** The authors declare that they have no competing interests. **Data and materials availability:** The murine and human datasets (scRNA-seq and snATAC-seq) generated in a previous study are deposited in the Gene Expression Omnibus (GSE151962, GSE152011, and GSE178454) (*23*, *26*). All data needed to evaluate the conclusions in the paper are present in the paper and/or the Supplementary Materials.

Submitted 13 July 2021
Accepted 19 October 2021
Published 15 December 2021
10.1126/sciadv.abl4391